# LEFT VENTRICULAR VOLUME ESTIMATION FROM RADIONUCLIDE IMAGES USING AN ELLIPSOIDAL MODEL



COLIN L. AU

# Left Ventricular Volume Estimation From Radionuclide Images Using An Ellipsoidal Model

By

© Colin L. Au, B. Eng.

A Thesis submitted to the School of Graduate

Studies in Partial Completion of the Requirements

for the Degree of Master of Engineering

Faculty of Engineering and Applied Science

Memorial University of Newfoundland

St. John's, Newfoundland, Canada

July 1997

# Abstract

This thesis presents a method of left ventricular (LV) volume estimation that is an improvement over existing methods. The author has developed a method of left ventricular volume estimation using an ellipsoidal model. It is shown, in this thesis, that the volume of an ellipsoid can be estimated from three planar projections (radionuclide images). Thus, this method can be applied to estimate the volume of the left ventricle from three radionuclide images, taken at different angles. Left ventricular radionuclide images are formed when a radioactive source is injected into a patient. Generally, a patient's red blood cells are labelled with technetium $^{99m}Tc$ which will emit gamma ($\gamma$) rays during radioactive decay.

Two methods have been developed to estimate left ventricular volumes from these radionuclide images. Count based methods use the principle that the number of $\gamma$ rays detected over a surface is proportional to the volume of the source located under that surface. Geometric methods rely on the outline of the left ventricle and the accuracy heavily depends upon how well the geometric model fits the left ventricle.

To test the accuracy of using this geometric method, hollow ellipsoidal models were constructed. A total of 20 trials were performed in which the models were arbitrarily located relative to a fixed reference frame. Each image from the $\gamma$ camera (elliptic in shape) was then analyzed to determine the axes lengths and angle of rotation. The estimated volumes were compared with the theoretical volume and the percentage discrepancies ranged in magnitude from 0.7% to 13.9%.

One problem is that it may be difficult to determine the exact location of the left ventricular projection border because of scattering, interference of radiation from other organs, and pixel size (resolution of 6.13 $mm$/pixel). This problem can be minimized by selecting a certain count threshold to help determine where the left ventricular border is located. Another problem of using a geometric method of volume estimation is how well the geometric model fits the actual organ. For most cases, an ellipsoidal model does seem to be a relatively accurate model but abnormalities in the left ventricle will affect the accuracy.

It was discovered that self attenuation caused the observed counts to differ by as much as 33.7% for images within the same trial. If a count based left ventricular volume estimation method was performed on this same set of images, then there would be a relatively large discrepancy among the volume estimates. Because of so many factors such as attenuation, self attenuation, radioactive decay, scattering, and interference from other organs, it would appear as though count based methods would not be able to estimate accurately the volume of the left ventricle.

# Acknowledgements

The author would like to thank Dr. Carl Wesolowski (Director of Nuclear Medicine, General Hospital, St. John's, Newfoundland), Dr. John Quaicoe (Faculty of Engineering, Memorial University of Newfoundland), and Dr. Rod Donnelly for their guidance and assistance in the production of this thesis.

# Contents

# List of Figures and Tables

# Chapter 1:
# Introduction and Literature Review

This chapter will present an introduction to this thesis. Background information about the heart is presented followed by a description of how radionuclide images are formed. Different methods of left ventricular volume estimation will be discussed. A literature review outlining the variations of these methods will be presented. This should give an understanding of what has been done in the area of left ventricular volume estimation from radionuclide images. Due to the large quantity of papers that has been published in this area, only selected papers are discussed. An analysis of these papers and how the methods can be improved is also presented.

## 1.1 Introduction

The human heart is made up of four chambers: left and right atrium along with the left and right ventricle (Figure 1). During the cardiac cycle, the heart undergoes various phases which relate to the volume of the left ventricle (LV). During the contraction phase (systole), the ventricle ejects the blood. At the end of this phase, the left ventricular volume is minimal. The next phase is a relaxation phase (diastole) during which the ventricle fills. At the end of diastole, the left ventricular volume is maximum (Figure 2).

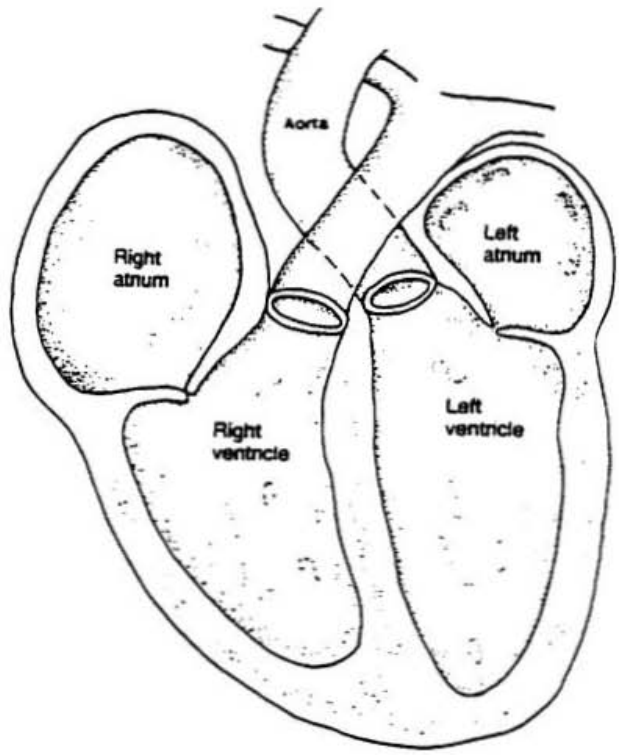


Figure 1: Interior view of the cardiac chambers (Phillips and Feeney, 1990).

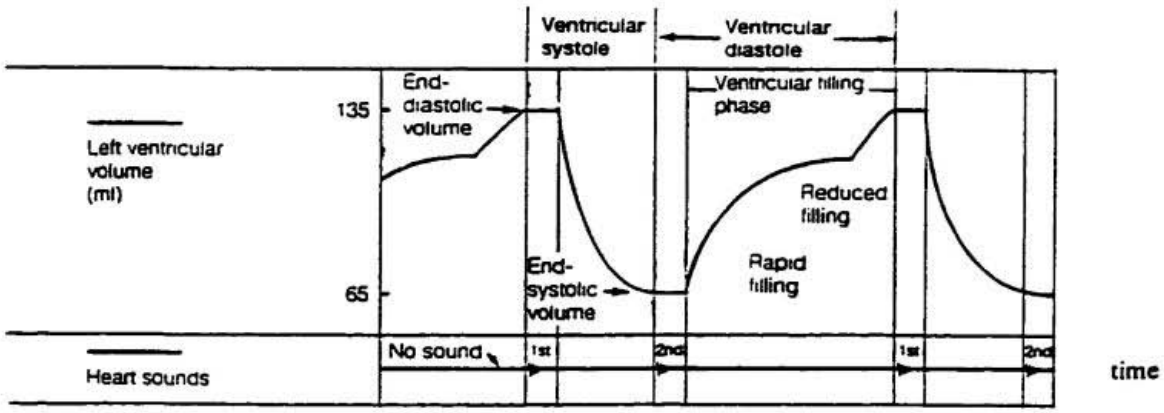


Figure 2: Left ventricular volume during the cardiac cycle (Sherwood, 1993).

Preliminary data suggest that left ventricular volume measurements provide prognostic information for patient survival. Various methods exist to obtain an estimate of the left ventricular volume, but many methods are not acceptable because of their inaccuracies and/or their invasive nature. Existing methods, within the area of nuclear medicine, are becoming popular because of their non-invasive nature.

Radionuclide images are formed when a radioactive source is injected into a patient (Figure 3). Generally, a patient's red blood cells are labelled with technetium $^{99m}Tc$ which will emit gamma ($\gamma$) rays during radioactive decay. The $\gamma$ rays are detected with a $\gamma$ camera and the position of the $\gamma$ ray, energy, and timing relative to the cardiac cycle are all used in the formation of images. Multiple images will then form a series representing the entire cardiac cycle. In order to obtain more accurate images of the organ, a parallel hole collimator is used with the camera. This device helps reduce the amount of scattering

by allowing only rays that are approximately parallel to enter the camera. Due to a finite hole diameter and length, each hole will have an acceptance angle which is usually only several degrees. After imaging has been completed, the images are processed using various analytical techniques. Two methods have been developed to estimate LV volumes from these radionuclide images. Count based methods use the actual number of $\gamma$ rays (counts) whereas geometric methods rely on the outline of the left ventricle.

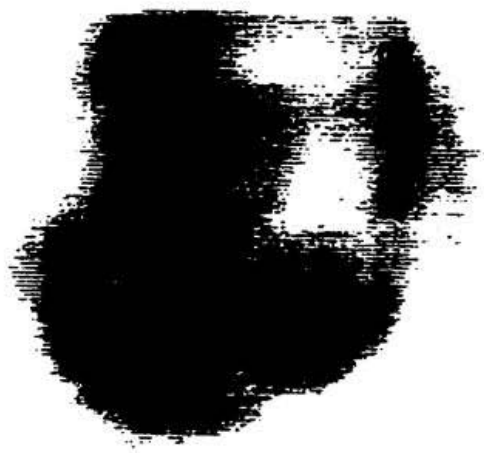

Figure 3: Radionuclide image of the heart.

Count based methods use the principle that the number of $\gamma$ rays detected over a surface is proportional to the volume of the source located under that surface. In theory, the number of counts is directly proportional to the volume if 1) the source is emitting $\gamma$ rays at a constant rate, 2) the source is homogeneous, 3) the attenuation is constant over the entire surface, and 4) the distribution of background activity is constant over the entire surface. In reality, none of the above conditions hold, but in practice conditions 1) and 2) can be

assumed. The issue of attenuation has been studied by several authors. Their findings suggest that attenuation corrected data leads to more reliable estimates of LV volumes than using data without attenuation correction. The amount of background activity is another important aspect of count based methods because most studies have taken approximately half of the total number of counts to be background. The large percentage of counts due to background raises serious concerns of how accurate this radionuclide method of left ventricular volume estimation could be. It should be noted that several papers have discussed background counts but there has been no concensus on how to determine the amount of background.

Geometric methods do not have the problems of attenuation and background determination. However, the background activity does make it difficult to locate the left ventricular border. The accuracy of this method heavily depends upon how well the geometric model fits the left ventricle. Even with simplistic models such as a sphere or a prolate spheroid, results have been relatively accurate (Greene *et al.* 1967 and Massardo *et al.* 1990).

## 1.2 Literature Review

This section presents a review of methods used to estimate LV volumes. Several authors (Rackley 1976, Ashburn *et al.* 1978, Strauss *et al.* 1979, Massie *et al.* 1982, Slutsky 1983, Al-Khawaja *et al.* 1988, Clements *et al.* 1990, Aurigemma *et al.* 1995) have reviewed much of the research performed in this area. This section shall elaborate on these papers while reviewing the work of other researchers. The papers are presented in chronological order which should show the progression of methods. A discussion of the various problems associated with these methods are presented at the end of this chapter. This will reduce the repetition of restating the same problems associated with many papers. Also, it will be shown how this earlier work will be improved upon in the method developed in this thesis.

Dodge *et al.* (1960) studied the use of biplane angiocardiography for the measurement of LV volume. Using an ellipsoidal model, LV volume can be estimated by determining the three axis dimensions. They correctly point out that unless a given axis is parallel to the filming plane, it cannot be measured directly. They point out that a minor axis length can be calculated from the formula for the area for an ellipse since the projection of an ellipsoid is an ellipse (Arvidsson, 1958). They obtained excellent correlations for the various methods tested (spatial, longest measured length, three measured lengths, area product, and Simpson's rule). Kennedy *et al.* (1970) compared anteroposterior (AP) and right anterior oblique (RAO) methods with biplane angiocardiograms to determine LV volumes. For the single plane methods, they used the method described by Dodge

*et al.* (1960) for an ellipsoidal model in which the short axis dimension was derived from the area and length. Both AP and RAO methods had the same correlation results with biplane values (correlation coefficient $r = 0.97$, standard error of estimate $SEE = 24\ mL$) but RAO volumes substantially overestimated the biplane values ($y = 0.81x + 1.9$). Hillis *et al.* (1984) assessed the accuracy and reliability of the regression equations of Kennedy *et al.* (1970) and Wynne *et al.* (1978) as applied to LV volume estimates using the method described by Dodge *et al.* (1960). Scintigraphic/thermodilution determined volumes correlated well with the Kennedy regression ($r = 0.95$, $SEE = 8.1\ mL$, $y = 0.99x$) and the Wynne regression ($r = 0.95$, $SEE = 9.8\ mL$, $y = 1.17x - 5.5$).

Davila and Sanmarco (1966) analyzed the fit of mathematical models applicable to the measurement of LV volume. Postmortem hearts from 23 normal adults were studied. The correlation coefficients were good for all models ($0.908 - 0.983$) for both photographs and radiographs. The best results were obtained with models that divided the left ventricle into many cylindrical sections and also with ellipsoidal models in which the minor axis dimensions were estimated from the area. Measurement of all three dimensions for an ellipsoidal model gave less accurate results.

Greene *et al.* (1967) performed single plane cineangiography to estimate LV volumes. They simplified the method of Arvidsson (1958) by assuming that the two minor axis lengths were equal (prolate spheroid model). The two unknown dimensions could then be measured from one view if the major axis was parallel to the filming plane. With the use of biplane measurements, they found that the two minor axis lengths differed by only a small amount in most cases ($r = 0.993$, $y = 0.993x - 0.305$) with the extreme ratios of 0.79

and 1.02. The mean of the ratios was 0.93. Their method overestimated LV volumes in postmortem hearts. Sullivan *et al.* (1971) compared geometric radionuclide LV volumes to contrast angiographic results by using the method described by Greene *et al.* (1967) for an ellipsoid model ($V = \pi LD^2/6$) on radionuclide and contrast images. They obtained a good correlation between methods ($r = 0.9$, $y = 0.917x - 1.729$).

Slutsky *et al.* (1979) described a count based method to determine LV end diastolic (ED) and end systolic (ES) volumes from gated equilibrium studies. Several equations were used to express volumes in nondimensional units and in milliliters. The administered dose and radioactive decay were accounted for in some of these equations. In this study, the effects of attenuation and decay were not significant with the phantom (constructed model of the left ventricle) data. Patient studies were used to compare this count based method with contrast angiography by applying a regression equation ($r = 0.90$, $y = 0.14x + 3.12$). Maurer *et al.* (1983) showed that the attenuation can vary significantly from one patient to another. Thus, using a regression analysis will not be as accurate as using individual attenuation correction since a regression equation will correct for the average attenuation of the study group.

Slutsky *et al.* (1980) evaluated a method of obtaining LV volume estimates from gated equilibrium radionuclide studies by counting the blood sample $\gamma$ rays with the scintillation camera. They compared this counting method to using a well counter. The volume estimates correlated well with contrast angiographic results for both well counting ($r_{ED} = 0.94$, $r_{ES} = 0.95$) and for camera counting ($r_{ED} = 0.93$, $r_{ES} = 0.94$). A test tube containing the blood sample was placed upright over the camera so that there was

significant self attenuation. Also, regression analysis was used to convert the radionuclide volume units to absolute units.

Dehmer *et al.* (1980) estimated LV volumes using a nongeometric method applied to gated equilibrium blood pool scans. Background activity was determined by comparison of horizontal count profiles at three levels through the LV in the end diastolic frame. The point where the three curves intersect outside the LV was taken as the background activity. A regression analysis was performed with contrast angiography to convert the attenuated radionuclide units to absolute volume units at end diastole ($r = 0.985$, $SEE = 16.2\ mL$, $y = 6.08x - 23.3$) and at end systole ($r = 0.988$, $SEE = 14.7\ mL$, $y = 6.24x - 10.13$). Using an average attenuation correction (regression analysis) will be less accurate than using individual attenuation correction because of the variation in attenuation from patient to patient.

Dehmer *et al.* (1981) calculated LV volumes from gated equilibrium blood pool studies using the method described by Dehmer *et al.* (1980) with a modification in the determination of background. A previously determined regression equation ($y = 4.98x + 6.9$) developed by Lewis *et al.* (1979) was used to compensate for decreased counts due to attenuation. The background image was determined by manipulations of the end diastolic frame. A rectangle was drawn over the heart so that all cardiac chambers were included. Along each row of the rectangle, each pixel was reset to a weighted average (relative to distance) of the three pixel average to the left and right of the rectangle. Correlation was made with angiogram results at end diastole ($r = 0.86$, $SEE = 2.7\ mL$, $y = 0.78x + 26$) and at end systole ($r = 0.73$, $SEE = 7.2\ mL$, $y = 0.57x + 18$). Dependence on a regression

limits the accuracy and reliability of this method which could account for the relatively poor correlation with angiography.

Clements *et al.* (1981) estimated LV volumes by using a pre-determined regression equation. A background region of interest (ROI) was selected from an area posterior and lateral to the LV at end systole. LV borders were found by a semiautomated edge detection program. They assumed that attenuation was constant and independent of the patient. A regression equation ($y = 3.54 \times 10^4 x - 45.6$) was used to relate counts to contrast angiographic volumes. Correlations were good at end diastole ($r = 0.87$) and at end systole ($r = 0.95$). This regression equation was then used in other studies. The correlations with contrast results were excellent but the slopes were far from identity (0.60 for end diastole and 0.66 for end systole). Because attenuation can vary significantly between individuals (Maurer *et al.*, 1983), the use of a regression equation will introduce errors. This may explain why the correlation with contrast angiographic volumes did not yield slopes close to unity.

Hutton *et al.* (1981) presented a method to determine LV volumes by considering a bolus. It is assumed that the complete bolus passes only once through the ventricle and that perfect mixing of tracer occurs in both the left ventricle and the atrium. The area under the first pass count rate versus time curve will be proportional to the activity and the mean residual time. The constant of proportionality will represent the attenuation factor.

Iskandrian *et al.* (1981) compared radionuclide and catheterization LV volume measurements. They used the geometric method of Dodge *et al.* (1962) for an ellipse of

revolution to estimate the radionuclide LV end diastolic volume. There was good correlation between the methods for estimating end diastolic volumes ($r = 0.94$, $y = 0.81x + 46$).

Parrish *et al.* (1982) assessed radionuclide ventriculography for right and left ventricular volume estimation in children. Count based and geometric methods were used to determine ventricular volumes and the results were compared with cineangiographic results. The chest wall thickness was calculated from a regression line since it was too inaccurate to measure it using a technetium marker. An attenuation coefficient of 0.1 $cm^{-1}$ was assumed. An area-length method was used for the left ventricle (Graham *et al.*, 1971) while Simpson's rule was applied to the right ventricle (Graham *et al.*, 1973). Correlations were excellent at end diastole for the geometric method ($r = 0.97$, $SEE = 23\ mL$, $y = 1.1x - 14.3$) and for the attenuation correction method ($r = 0.93$, $SEE = 25.4\ mL$, $y = 0.79x$). Correlation was poor without attenuation correction ($r = 0.86$, $SEE = 12.8\ mL$, $y = 0.28x + 6.2$). They proposed four regression equations for count based and geometric methods applied to the left and right ventricles.

Massie *et al.* (1982) compared geometric and count based methods using data from first pass and equilibrium blood pool scintigraphy. Both methods had good correlations with contrast angiography but count based was better because of a smaller variance. Various geometric methods were studied. Using the count based method, they found that the 95% confidence limits of the measurements were narrow enough to reliably discriminate between small, normal and enlarged ventricles. They also found that self attenuation within the blood pool was not important which agreed with some findings (Slutsky *et al.* 1980 and Dehmer *et al.* 1980) but disagreed with others (Strauss *et al.*, 1979).

Nickel *et al.* (1982) found a relationship between the normalized total count rate (total count rate divided by the maximum count density) and the volume. Using balloons of various sizes located at different distances from the collimator, they found a linear relationship between the normalized total count rate and the volume. For patient studies, they applied background subtraction and then estimated LV depth to calculate LV volumes using their determined relationship. Background was modelled as a linear relation to the measured lung distribution. LV depth was estimated using an experimentally derived formula that related depth to projection angle, weight and height. They obtained good correlation with angiographic volumes ($r = 0.95$, $y = 1.04x - 3.13$). Some error may result from determining the relationship while imaging balloons with the major axis parallel to the image plane. The major axis of the LV will be approximately perpendicular to the image plane in the left anterior oblique (LAO) view.

Links *et al.* (1982) measured LV volume from gated blood pool studies and compared the results with single-plane contrast ventriculography. The ratio of attenuation corrected counts to the counts per milliliter from a blood sample yielded the LV volume. The attenuation correction factor, $e^{-\mu d}$ was estimated by using $\mu = 0.15\ cm^{-1}$ (narrow beam attenuation coefficient for water) and using a skin marker to measure $d$, the distance from the center of the LV. They imaged the blood samples using a test tube and a petri dish to show the effect of self attenuation. The petri dish samples averaged approximately 20% more counts than the test tube samples. Semi-automatic ROI's were generated over the LV using a combined second derivative and count threshold algorithm. The background ROI was automatically generated lateral and inferior to the LV in the end diastolic frame,

five pixels wide and two pixels from the LV edge. After generation of a time activity curve, the end diastolic, end systolic and background ROI's were manually drawn. These regions were purposely drawn large especially near the free wall but care was taken to exclude the left atrium, right ventricle and other major vascular structures. The gross LV end diastolic counts averaged 93 counts/pixel while the background averaged 45 counts/pixel. They correctly point out that not accounting for the effect of self attenuation introduces a very small error for a prolate spheroid with its major axis perpendicular to the viewing direction and with a minor axis of 5 *cm* or less. But for views that are not perpendicular to the major axis, the error will be more significant. In fact, the larger the angle between the major axis and the plane of the camera face, the larger the error due to self attenuation. For larger angles, there will not only be significant self attenuation but also body attenuation of various amounts because of different distances between volume elements of blood and the chest wall. They obtained very good correlations for both phantoms and patient studies. They obtained better results with attenuation correction compared to using a regression equation. They found that a change in the depth of 0.36 *cm* (one pixel) caused a change in volume of 5%. Melin *et al.* (1985) used the method descibed by Links *et al.* (1982) to compare radionuclide and Fick cardiac output measurements. There was some correlation of the cardiac outputs ($r = 0.904$, $SEE = 1.77\ mL$, $y = 0.70x + 1.43$) and the stroke volumes ($r = 0.642$, $SEE = 13.88$, $y = 0.51x + 33$) but the radionuclide values were significantly lower than the Fick measurements. Burow *et al.* (1982) assessed the ability to determine stroke volumes by using the method described by Links *et al.* (1982). They also studied the effect of attenuation correction. The correlation with thermodilution was

better with attenuation correction ($r = 0.96$, $SEE = 6\ mL$, $y = 0.99x + 1.2$) than without ($r = 0.80$, $SEE = 12\ mL$, $y = 2.31x + 18$).

Seldin *et al.* (1983) evaluated a semi-automated geometric method to obtain LV volumes from gated blood pool studies. An end diastolic ROI was drawn by a semi-automatic edge detection algorithm from which a larger ROI was then created since such regions have been shown to under estimate the true chamber borders as described by Links *et al.* (1982). Images were taken in the LAO projection and foreshortening of the major axis was minimized by a caudal tilt. Volumes were then calculated by the formula of Sandler and Dodge (1968), $V = 8A^2 \ / \ (3\pi L)$. Correlation with contrast ventriculography was moderate at end diastole ($r = 0.93$, $SEE = 36\ mL$) and at end systole ($r = 0.95$, $SEE = 35\ mL$). Having the major axis not parallel to the image plane can cause significant errors since it will decrease both $A$ and $L$.

Burns *et al.* (1983) examined the repeatability of LV volume estimates from blood pool counts. They studied interpatient and intrapatient variability of the in vivo half life of $^{99m}Tc$ labelled red blood cells. They found a mean in vivo half life of 4.1 hours which is quite different to the physical half life of 6 hours. Their results also indicate significant interpatient ($0.9 \pm 0.8$ hours) and intrapatient ($1.0 \pm 0.9$ hours) variability which agreed with previous findings (Eckelman *et al.* 1975 and Ryo *et al.* 1976). This variation in half life can affect the results of gated equilibrium studies performed over a long period of time especially if blood sample counts are corrected for decay.

Maurer *et al.* (1983) estimated LV volumes from gated blood pool images using an in vivo point source to correct for attenuation. A capsule containing a calibrated dose

of $^{99m}Tc$ was attached to a thread and imaged behind a phantom to avoid saturation. The capsule was then swallowed by the patient and imaged as it descended the esophageal tube. Increased attenuation and a 40 *cm* mark on the thread were used to indicate when the capsule was behind the LV. When the capsule reached the stomach, the patient's red blood cells were labelled with $^{99m}Tc$. They obtained good correlations with contrast ventriculography using both Simpson's rule and the area-length method. The attenuation factors ranged from 0.11 to 0.35 with an average of 0.21. These factors represent the reciprocal of the slope for the regression equation of each individual patient. Regression data from Slutsky *et al.* (1979), Dehmer *et al.* (1981), and Links *et al.* (1982) yielded attenuation factors of 0.13, 0.16, and 0.29, respectively. But these values represent the average attenuation factors of the patient group. The wide range of values will certainly contribute to an erroneous volume estimate if an average attenuation factor is used instead of individual ones. This may account for why Links *et al.* (1982) obtained better results with individual attenuation correction as compared to using a regression equation.

Harpen *et al.* (1983) determined LV volumes by analyzing the first pass kinetics of labelled red blood cells. They obtained a relationship between the total amount of bolus activity, ejection fraction and total counts. The attenuation factor can then be calculated by dividing the total activity of the bolus by the total activity injected into the patient. Manual ROI's were drawn over the LV with the background area drawn on the end systolic frame. They obtained excellent correlation with contrast ventriculographic volumes ($r = 0.98$, $y = 0.987x + 1.76$).

Thomsen *et al.* (1983) calculated LV volumes by using two dimensional echocardiog-

raphy to estimate LV depth. Automatic ROI's were generated and a Fourier phase image was used to avoid excluding LV counts. A semi-automatic background ROI was generated at end systole. The background ROI consisted of an area two pixels wide and covered an arc of 60 deg. The lowest mean counts per pixel for background ROI's between one and seven o'clock was chosen. They obtained excellent correlation with contrast volumes for end diastole ($r = 0.94$, $S_{yx} = 20.6\ mL$, $y = 0.92x + 18.1$) and end systole ($r = 0.95$, $S_{yx} = 16.6\ mL$, $y = 0.98x - 4.5$). Using only the depth from the geometric center of the LV will result in an overestimation of the attenuation.

Seiderer *et al.* (1983) studied the influence of background and absorption correction on LV end diastolic volume quantification. Thoracic and heart wall absorption, self absorption, and background were all considered in converting counts to milliliters. Three background models (uniform, parabolic, and no background) were investigated. In the parabolic model of background, the counts ranged from zero to the level in the background ROI. To calculate the amount of self absorption, they assumed that the LV depth was 1.5 times the maximum ventricular width vertical to the major axis in the end diastolic ROI. They chose a ratio of 1.5 instead of 2.0 for the heart model of the Medical Internal Radiation Dose Committee (Coffey *et al.*, 1981) since it would be less sensitive to the projection angle and enlarged ventricles. A smaller ratio of axes would also be needed if the LV was not viewed directly along the major axis but it is difficult to quantify the exact ratio since it is dependant upon the angle between the major axis and the view direction. They obtained the best correlation and line of identity as compared to single plane cineventriculography when using parabolic background subtraction.

Nickoloff *et al.* (1984) studied the attenuation of $\gamma$ rays by body tissue that is relevant in LV volume estimation. They estimated the attenuation coefficient for the 40° LAO view to be about 0.13 $cm^{-1}$ from computed tomography scans.

Høilund-Carlsen *et al.* (1984) determined LV volumes by estimating individual attenuation factors. They placed two radioactive markers exactly 9 $cm$ apart over the left ventricle. The depth of the left ventricle was determined and compared with the depth measured by echocardiography. There was no statistical difference between the depths measured by these two methods. The attenuation coefficient for ball shaped phantoms immersed in water at various depths was determined to be approximately 0.156 $cm^{-1}$ with little variation for different sized balls (36.7 $mL$ - 192.4 $mL$). The background ROI was defined from the mean activity in an area near the LV with minimal activity over three successive systolic frames. They obtained excellent correlation with thermodilution at end diastole ($r = 0.96$, $SEE = 27\ mL$, $y = 1.06x - 14$) and at end systole ($r = 0.98$, $SEE = 20\ mL$. $y = 1.05x - 6$). Using the depth from the chest wall to the geometric center will not accurately represent the attenuation depth when the LV major axis is almost perpendicular to the image plane.

Siegel *et al.* (1984) obtained absolute LV volumes by using an iterative build-up factor analysis. The build-up factor accounts for the increased counts due to a broad beam geometry when using a narrow beam attenuation coefficient. Images were acquired from two views 180° apart: LAO and right posterior oblique (RPO). They derive a relationship between the measured counts, build-up factor, unattenuated counts, depth attenuation, and self attenuation. Once the unattenuated count rate is solved for by an iterative method,

absolute volumes are calculated by comparing it to a blood sample count rate. An end diastolic ROI was generated on the LAO image using a second derivative and count threshold algorithm. Background was chosen in an area next to the ventricle in the end diastolic frame. A manual ROI was drawn on the RPO image at end diastole with the aid of first pass images to identify the LV. They obtained good correlation with angiographic results at end diastole ($r = 0.97$, $SEE = 17.1\ mL$, $y = 0.94x + 3.7$). The use of constant background subtraction and discrepancies between the LV outline on both views may introduce some error.

Rabinovitch *et al.* (1984) analyzed the inherent errors of LV volume measurement from gated equilibrium blood pool scintigraphy. They used computer generated regions of interest for the LV and background. Some modification was necessary to prevent selection of the aorta and spleen in the background ROI which was drawn on the end systolic frame. Counts were corrected for dead-time losses and attenuation. The average background counts were approximately 50% of the average raw counts for end diastole and end systole. Various attenuation coefficients ($\mu$) were evaluated. The highest correlation and smallest standard error of estimate were obtained when $\mu = 0.10\ cm^{-1}$ for end diastole and $\mu = 0.12\ cm^{-1}$ for end systole. The combined count threshold second derivative edge detection program used in this study excluded some LV counts. Attenuation correction only marginally improved the correlation with contrast volumes but relying on a regression equation can produce poorer results as demonstrated by Dehmer *et al.* (1981).

Schwaiger *et al.* (1984) used a bolus to estimate the amount of attenuation and then used the result to determine LV stroke volumes from gated pool studies. A cresent shaped

region was drawn at end diastole to determine the background activity. In comparing stoke volumes obtained by thermodilution and their attenuation corrected count based method, they found that using individual attenuation correction ($r = 0.92$, $SEE = 6.1\ mL$, $y = 0.9x + 4.4$) was significantly better than using the mean attenuation factor ($r = 0.52$, $SEE = 14.8\ mL$, $y = 0.57x + 25.8$). They also found a correlation between both body weight and body surface area to the measured attenuation factor. The use of an invasive method to determine individual attenuation factors limits the acceptability of this approach.

Petru *et al.* (1984) evaluated ventricular function estimation by comparing attenuation corrected radionuclide angiography with contrast angiography and the Fick technique. The distance between the center of the LV and the chest wall was measured using the same technique as that of Links *et al.* (1982). They used uniform background subtraction and assumed that the attenuation coefficient was 0.16 $cm^{-1}$. Fluoroscopy was used to verify the ventricular depth calculations in some patients. Cardiac outputs determined by the Fick technique correlated well with those determined by radionuclide angiography, with and without attenuation correction. There was some correlation between radionuclide and contrast angiographic LV volumes but the standard error of estimate was high and interestingly the radionuclide technique seemed to be overestimating the volume. This overestimation occurred mainly in patients with abnormal wall motion.

Nichols *et al.* (1984) estimated LV volumes without the need of measuring LV depth or regression equations. By viewing the LV at two different views 90° apart, a relation between counts and voxels (volume elements) can be calculated. A background ROI, two

pixels beyond the border was drawn between the three and five o'clock positions on the end systolic frame. They obtained excellent results with phantoms ($r = 0.999$, $SEE = 15\ mL$, $y = 0.96 + 7.9$) and with patients for end diastole ($r = 0.96$, $SEE = 14\ mL$, $y = 0.97x + 8$) and for end systole ($r = 0.98$, $SEE = 11\ mL$, $y = 1.05x - 1$) with thermodilution as the reference. They showed that the effect of self attenuation for a sphere produces a small error. This error may be larger though for an ellipsoid or prolate spheroid which is a more representative model of the left ventricle. Calculating the count density from counts in only one pixel could also cause some error because of the statistical nature of the $\gamma$ ray count distribution.

Starling *et al.* (1984a) used a simple geometric attenuation correction to obtain accurate estimates of absolute LV volumes from radionuclide count data. They determined the distance from the center of the LV to the chest wall by placement of a technetium marker based on anatomic landmarks on two separate views (Berman *et al.*, 1975). An attenuation coefficient of 0.15 $cm^{-1}$ was assumed. They found that semi-automated ROI's were too small and thus under estimated LV volumes at end diastole ($r = 0.96$, $SEE = 31\ mL$, $y = 0.95x - 21$) and at end systole ($r = 0.97$, $SEE = 24\ mL$, $y = 1.03x$).

Starling *et al.* (1984b) examined the importance of attenuation correction for estimating LV volumes by equilibrium radionuclide angiography. Attenuated and attenuation corrected results were compared with biplane contrast cineangiography LV estimates. Attenuation correction was performed as described by Starling *et al.* (1984a). Attenuation corrected results ($r_{ED} = 0.96$, $r_{ES} = 0.98$) correlated better than the attenuated estimates ($r_{ED} = 0.74$, $r_{ES} = 0.87$). Individual correction is much better than using an average at-

tenuation correction (regression equation) because the amount of attenuation can vary significantly from one patient to another as shown by Maurer *et al.* (1983).

Burns *et al.* (1985) estimated LV volumes from attenuation corrected counts by using a modification of the triangulation method of Links *et al.* (1982). ROI's were determined with a semi-automated second derivative edge detection algorithm. An average attenuation coefficient ($\mu = 0.163\ cm^{-1}$) was independently determined from thermodilution volumes and radionuclide counts in eight other patients. There was good correlation with contrast volumes ($r = 0.96$, $SEE = 15.8\ mL$, $y = 1.3x - 39.8$). Volume estimates from patients with normal wall motion were better than results from patients with abnormal wall motion. Inaccuracies from the depth measurement, attenuation coefficient, and the effect of self attenuation are potential sources of error.

Fearnow *et al.* (1985) examined factors that affect ventricular volume determination from a count based equilibrium method. Using a spherical source in an elliptical torso phantom, they analyzed the effect of source depth, ROI size, background concentration, and source shape on volumes determined by using an attenuation correction count based method described by Jaszczak *et al.* (1980) and Links *et al.* (1982). They found that the estimated volume of the 96 $cm^3$ source decreased linearly as the background concentration increased ($r = 0.97$, $y = -5.3x + 95$). However, if the volume of the source is taken into consideration during background subtraction then the estimated volume remains constant at about 95 $cm^3$. Imaging cylindrical sources resulted in accurate volume estimations but the cone shaped sources resulted in significant errors especially when using the depth to the linear center instead of the geometric center. Their results indicate that there are many

possible sources of error in determining count based ventricular volumes. Of particular importance is the effect of background subtraction since background can account for about half of LV counts.

Verani *et al.* (1985) estimated LV volumes using an attenuation coefficient derived for a broad beam geometric model. Using phantoms immersed in water at different depths, they found that the attenuation coefficient was 0.144 $cm^{-1}$. The radionuclide volumes were higher than the true balloon volumes, particularly for larger volumes. This is probably due to using an average depth which over estimates the attenuation and thus over estimates the true volume. They measured LV depth by imaging a radioactive marker in a different view. They obtained good correlation with contrast volumes for end diastole ($r = 0.98$, $SEE = 16.4\ mL$, $y = 1.009x$) and for end systole ($r = 0.95$, $SEE = 17.1\ mL$, $y = 1.037x$). They also showed that changing the value of the background level caused significant changes in the volume estimates.

Simon *et al.* (1985) studied the effect of self attenuation on left and right ventricular volume estimation using realistic cardiac phantoms. Using four different sized phantoms, they found excellent correlation between scintigraphic estimates and the true volume. Correlation between angiographic volumes and the true volumes were also excellent. They imaged the phantoms in the LAO view, perpendicular to the interventricular septum. Their results showed that the effect of self attenuation can be ignored for $^{99m}Tc$ studies in the volume range encountered clinically. But they did not study the effect of viewing the LV with the major axis tilted towards or away from the camera. This will increase the significance of self attenuation and the importance of non-uniform attenuation because of

varying distances from the chest wall.

Koral *et al.* (1985) examined the effects of various parameters on LV volume estimation using a radionuclide count based method. They studied two methods of calculating LV depth, the use of one or two attenuation coefficients, optimization of attenuation coefficient(s), and an automated program for expansion of the ROI. Depths were determined by measuring the distance from the midpoint between the mitral valve plane and the apex of the LV to the chest marker and also by a count weighted formula. They had the smallest scatter with $\mu = 0.10\ cm^{-1}$ for end diastole and $\mu = 0.12\ cm^{-1}$ for end systole. The reason why optimization appears to be occuring at different values of $\mu$ is probably because of the constant background subtraction. Perhaps a better model of background such as that used by Seiderer *et al.* (1983) would provide a better estimate of the attenuation coefficient.

Keller *et al.* (1987) studied the attenuation of $^{99m}Tc$ photons from a known source located at various sites within the heart. They found that for 36 patients, the regression line indicated an attenuation coefficient of 0.12 $cm^{-1}$ with a correlation of 0.93. The calculated values ranged from 0.8 $cm^{-1}$ (for the LV apex) to 0.13 $cm^{-1}$ (for the inferior vena caval/right atrial junction). However, there was no significant difference in the values of the attenuation coefficient from the four intracardiac sites. These results agree with the findings of other researchers such as Fearnow *et al.* (1985), Nickoloff *et al.* (1984) and Harris *et al.* (1984). If these findings are accurate, this would explain why several researchers have presented methods which over estimate LV volumes.

Boström *et al.* (1987) studied the effects of scattered radiation and background activity on radionuclide LV volume estimation using patients and phantoms. Using phantoms

without background activity, they confirmed that the depth correction factor decreased with respect to that expected for narrow beam geometry as used by Links *et al.* (1982). But with the addition of background having 10% of the activity of the phantoms, the depth correction factor increased. The overall effect caused the depth correction factor for a phantom with background activity to closely match that for narrow beam geometry. The absolute background counts depend on the activity and the depth of the background area. Thus, many combinations can simulate realistic background counts but each variation in background activity and depth causes the depth correction factor to change since the amount of background activity displaced by the LV will change. Perhaps a more realistic model of the background will reflect actual conditions and thus provide a better estimate of the depth correction factor. Rabinovitch *et al.* (1984) reported smaller attenuation coefficients.

Massardo *et al.* (1990) estimate absolute left ventricular volume using a count based ratio method applied to gated equilibrium studies. They assumed that the LV is spherical and derived a relationship between the volume, pixel area and ratio of total counts to maximum pixel count. They claimed that this relationship is valid for a chamber of any shape. This is obviously not true since one can consider a prolate spheriod and a sphere, each of the same volume. Viewing the spheriod along its long axis, the pixel area and total counts will be the same as that for the sphere but the maximum pixel count will be larger indicating a different volume. Their derivation did not consider the problems of attenuation and background which can certainly vary from pixel to pixel thus introducing more error.

Mahmarian *et al.* (1991) discussed the interpretation of changes in the left ventricular ejection fraction and cardiac volumes as assessed by rest and exercise gated radionuclide angiography. They tried to quantify the sources of variation associated with sequential radionuclide angiographic measurements. A lead marker was used to determine LV depth and thus the attenuation correction factor. All cardiac output and volume measurements were indexed to the body surface area. Nine point smoothing and background subtraction was performed as described by Verani *et al.* (1985). With a probability $\leq 0.05$ that the observed change was due to random variation, they found that a change was significant in rest studies for $\geq 7\%$ units for LV ejection fraction, $\geq 45\ mL/m^2$ for end diastolic volume, $\geq 35\ mL/m^2$ for end systolic volume, $\geq 20\ mL/m^2$ for stroke volume and $\geq 1.25\ L/min$ per $m^2$ for cardiac index. They also determined significant values in exercise studies. A larger population ($> 39$) of patients would certainly increase the reliability of the results but it might not be valid to use these results at other institutions where there are many different factors such as inherent system errors, variation in the count based technique, etc.

Sapin *et al.* (1993) compared three dimensional echocardiography, two dimensional echocardiography, and cineventriculography for the purpose of measuring LV volume. Excised hearts were prepared with an internal latex lining that could be filled with a known volume of liquid. LV volumes were calculated from 15 hearts at 25 volumes ranging from 50 to 280 $mL$. All methods tended to underestimate the true volume. There was a significant correlation between bias magnitude and volume size for the two dimensional echocardiography. The bias for the three dimensional echocardiography was fairly constant over the

range of volumes. When bias was accounted for, the results indicated that two dimensional echocardiography was significantly less precise than the other two methods tested in terms of percent error (two dimensional echocardiography $15.3 \pm 11.9\%$, three dimensional echocardiography $3.9 \pm 3.4\%$, and cineventriculography $5.6 \pm 5.7\%$).

Pattynama it et al. (1994) evaluated the performance of using magnetic resonance imaging (MRI) to determine cardiac function. The accuracy of MRI has been established by imaging a ventricular model of known volume (Longmore *et al.*, 1985) but in vivo MRI measurements have been validated in only a limited number of studies. A major problem is the choice of a gold standard. MRI measurements of ventricular volumes have been validated only with nonsimultaneously performed contrast ventriculography.

Chin *et al.* (1997) determined LV volume with tomographic gated equilibrium blood-pool scintigraphy (TMUGA) and compared it to MRI and conventional planar scintigraphy. The volume was calculated using a modified Simpson's rule which assumes that the LV has a shape similar to that of an ellipse of rotation. This method of volume determination showed good correlation with MRI ($r = 0.96$, $slope = 0.88$, $SEE = 18.2$). Further studies are needed to validate this method.

Table 1: Summary of various characteristics for different left ventricular volume methods.

| Author (reference) | t | r | bf | Reference Method | SEE (mL) | y=mx+b (m,b) |
|---|---|---|---|---|---|---|
| Dodge *et al.* (1960) | G | 0.98 | NA | Postmortem | | |
| Davila & Sanmarco (1966) | G | 0.91 | NA | Postmortem | | |
| Kennedy *et al.* (1970) | G | 0.97 | NA | Biplane Angio. | 24 | 0.81, 1.9 |
| Sullivan *et al.* (1971) | G | 0.90 | NA | Contr. Angio. | | 0.92, -1.7 |
| Slutsky *et al.* (1979) | C | 0.90 | | Contr. Angio. | | 0.14, 3.12 |
| Slutsky *et al.* (1980) | C | 0.94 | | Contr. Angio. | | |
| Dehmer *et al.* (1980) | C | 0.99 | ED | Contr. Angio. | 16.2 | 6.1, -23.3 |
| Dehmer *et al.* (1981) | C | 0.86 | ED | Contr. Angio. | 2.7 | 0.78, 26 |
| Clements *et al.* (1981) | C | 0.87 | ES | Contr. Angio. | | |
| Iskandrian *et al.* (1981) | G | 0.94 | NA | Catheter. | | 0.81, 46 |
| Links *et al.* (1982) | C | 0.95 | ED | Contr. Angio. | 36 | 0.97, 3 |
| Parrish *et al.* (1982) | G | 0.97 | NA | Cineangio. | 23 | 1.1, -14.3 |
| Nickel *et al.* (1982) | C | 0.95 | | Contr. Angio. | | 1.04, -3.13 |
| Maurer *et al.* (1983) | C | 0.96 | ES | Contr. Angio. | 21.2 | 0.99, 1.32 |
| Seldin *et al.* (1983) | G | 0.93 | NA | Contr. Angio. | 36 | |
| Harpen *et al.* (1983) | C | 0.98 | ES | Contr. Angio. | | 0.99, 1.8 |
| Thomsen *et al.* (1983) | C | 0.94 | ES | Contr. Angio. | 20.6 | 0.92, 18.1 |
| Høilund-Carlsen *et al.* (1984) | C | 0.96 | ES | Thermodil. | 27 | 1.06, -14 |
| Hillis *et al.* (1984) | G | 0.95 | NA | Thermodil. | 8.1 | 0.99 |
| Siegel *et al.* (1984) | C | 0.97 | ED | Contr. Angio. | 17.1 | 0.94, 3.7 |
| Petru *et al.* (1984) | C | 0.80 | | Contr. Angio. | | 1.24, -3.5 |
| Nichols *et al.* (1984) | C | 0.96 | ES | Thermodil. | 14 | 0.97, 8 |
| Starling *et al.* (1984a) | C | 0.96 | * | Contr. Angio. | 31 | 0.95, -21 |
| Burns *et al.* (1985) | C | 0.96 | * | Contr. Angio. | 15.8 | 1.3, -39.8 |
| Verani *et al.* (1985) | C | 0.98 | ES | Contr. Angio. | 16.4 | 1.009 |
| Massardo *et al.* (1990) | C | 0.95 | ES | Contr. Angio. | 23 | 0.94, 1.3 |
| Sapin *et al.* (1993) | G | 0.995 | NA | 3 D Echocard. | 7.1 | 1.02, 3.65 |
| Chin *et al.* (1997) | G | 0.96 | NA | Tomo. Gat. Sc. | 18.2 | 0.88, 14.1 |

Notes:

1. 't' indicates the type of analysis where
   G - geometric.
   C - count based.
2. 'r' is the correlation coefficient.
3. 'bf' stands for the background frame where
   ED - end diastolic  ES - end systolic  NA - not applicable
   * - more than one background frame used.
4. 'SEE' stands for the standard error of estimate.

Many methods of LV volume estimation have been developed over the past several decades. Most of these methods have inherent problems which should be addressed before using any of these methods. All of the previous methods can be grouped into the catagories of count based and geometric as indicated in Table 1. The problems of most of these methods can be discussed according to the inherent problems associated with each catagory.

All count based methods have the problem of significant background activity. Some reseachers (*e.g.* Links *et al.* 1982) were able to develop a way of removing the background counts but these techniques introduced errors. Subtracting an equal background count from the entire ROI assumes that the background is uniform. Studies have not been performed to validate this assumption. There are also the problems of scattering and attenuation which can significantly affect the counts in the ROI which directly influence the volume estimate. Links *et al.* (1982) also accounted for the attenuation and their method was accepted by many as the gold standard. This gold standard still contained inherent flaws which are associated with count based methods.

The geometric methods have several problems associated with them. Some researchers have used an ellipse of rotation or even a sphere (Massardo *et al.*, 1990) to model the LV. These geometric models are too simplified and an ellipsoid is more appropriate as shown by Davilla and Sanmarco (1966). Another problem is the border detection. Manually drawn borders have been effective but software programs have been developed to provide more consistency. If the LV is abnormal in shape, then even the ellipsoid model may not be accurate. Perhaps a hybrid of the geometric and count based methods can account for abnormalities and still provide a reasonably accurate estimate of the LV volume.

## 1.3 Thesis Objective

The objective of this research was to determine a method of estimating the volume of the left ventricle from radionuclide images. Several factors had to be taken into consideration while solving this problem of volume estimation. This method must be accurate. Cardiac volumes are used by medical doctors for prognosis of patients. This method must also be practical since it may be implemented in the future. In order to minimize the discomfort of the patient, this method should also be non-invasive. With consideration of the previously described methods, a geometric method using an ellipsoidal model was chosen for several reasons. A geometric method avoids the problems associated with count based methods. Also, the structure of the left ventricle resembles the shape of an ellipsoid (Davilla and Sanmarco, 1966). An ellipse of rotation (two axes lengths) would over simplify the left ventricle and would result in more error.

To determine the volume of an ellipsoid, it was necessary to study the projection of an ellipsoid onto a two dimensional plane. This projection would be similar to the radionuclide images formed during imaging of the left ventricle. If the volume of an ellipsoid can be determined from these projections, then left ventricular volumes can be estimated.

The next chapter will present the theory of this proposed method of volume estimation based on an ellipsoidal model. The experimentation along with results and discussion are then presented in chapter three. This chapter also discusses the importance of self attenuation, one of the main factors that limits the accuracy of count based methods. Finally, conclusions and recommendations are presented in chapters four and five.

# Chapter 2:
# Ellipsoidal Model for the Estimation of Left Ventricular Volume

This chapter will present the theory of determining the volume of an ellipsoid from planar projections. It is first necessary to determine the projection of an ellipsoid onto a two dimensional plane. This projection, which has been shown to be an ellipse, will be similar to the radionuclide images obtained during imaging of the left ventricle. Measurements of the major and minor axes along with the angle of rotation can be made from each projection. Several projections are required to provide the necessary equations needed to solve for the lengths of the ellipsoidal axes. These lengths can then be used to calculate the volume. The majority of the mathematical analysis performed in this chapter is original work done by the author.

## 2.1 Formulation of the Ellipsoidal Model

Consider an ellipsoid that is centered at the origin of a $xyz$ cartesian coordinate system (Figure 4). The projection of the ellipsoid onto any two dimensional plane will depend on three independent angular rotations. Without loss of generality, we can use the $xy$ plane as the projection plane. The orientation of any ellipsoid situated at the origin, with respect to the $xyz$ coordinate system, can be determined by three independent rotations about the $x$, $y$, and $z$ axes.

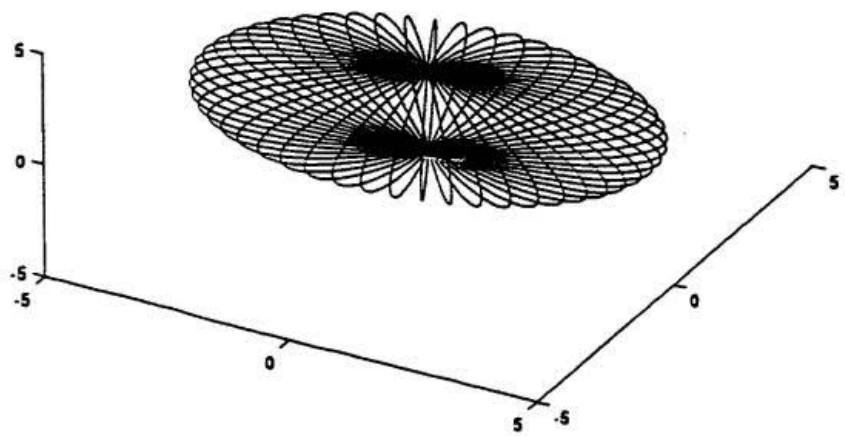


Figure 4: Ellipsoid centered at the origin without any rotation.

To accommodate these angular rotations, let us first rotate the $x$ and $y$ axes about the $z$ axis (counter clockwise as viewed looking towards the origin in the direction of the positive $z$ axis) by $\gamma$ radians to form the new coordinate system $\tilde{x}\tilde{y}\tilde{z}$, so the $\tilde{z}$ axis is the same as the $z$ axis. Next, we shall rotate the $\tilde{x}$ and $\tilde{z}$ axes about the $\tilde{y}$ axis (counter

clockwise) by $\beta$ radians to form the new coordinate system $\hat{x}\hat{y}\hat{z}$. Finally, we shall rotate the $\hat{y}$ and $\hat{z}$ axes about the $\hat{x}$ axis (counter clockwise) by $\alpha$ radians to form the new coordinate system $x_1y_1z_1$ (we can choose $\alpha$, $\beta$, and $\gamma$ such that the axes of any ellipsoid centered at the origin, with an arbitrary orientation, will lie along the $x_1y_1z_1$ axes). See Figure 5 for an arbitrarily rotated ellipsoid.

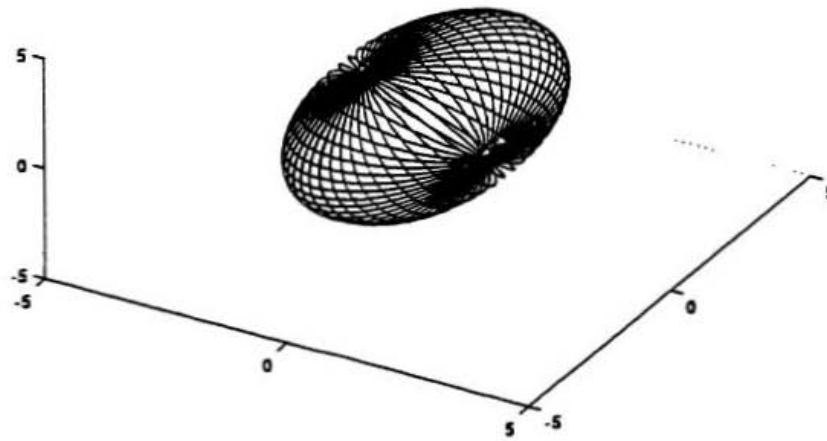


Figure 5: Ellipsoid arbitrarily rotated while centered at the origin.

A relationship between the $x_1y_1z_1$ coordinate system and the $xyz$ coordinate system can be found by considering how the new system was obtained from the original system. Using the following matrix definitions,

$$\mathbf{x} = \begin{pmatrix} x \\ y \\ z \end{pmatrix} \quad , \quad \tilde{\mathbf{x}} = \begin{pmatrix} \tilde{x} \\ \tilde{y} \\ \tilde{z} \end{pmatrix} \quad , \quad \hat{\mathbf{x}} = \begin{pmatrix} \hat{x} \\ \hat{y} \\ \hat{z} \end{pmatrix} \quad , \quad \mathbf{x}_1 = \begin{pmatrix} x_1 \\ y_1 \\ z_1 \end{pmatrix} \quad , \tag{1}$$

we can find a relationship between $\mathbf{x}$ and $\mathbf{x}_1$. Note that

$$\tilde{\mathbf{x}} = \mathbf{C}\mathbf{x} \quad , \quad \hat{\mathbf{x}} = \mathbf{B}\tilde{\mathbf{x}} \quad \text{and} \quad \mathbf{x}_1 = \mathbf{A}\hat{\mathbf{x}} \tag{2}$$

where

$$\mathbf{A} = \begin{pmatrix} 1 & 0 & 0 \\ 0 & \cos\alpha & \sin\alpha \\ 0 & -\sin\alpha & \cos\alpha \end{pmatrix} \quad , \quad \mathbf{B} = \begin{pmatrix} \cos\beta & 0 & -\sin\beta \\ 0 & 1 & 0 \\ \sin\beta & 0 & \cos\beta \end{pmatrix} \quad ,$$

$$\mathbf{C} = \begin{pmatrix} \cos\gamma & \sin\gamma & 0 \\ -\sin\gamma & \cos\gamma & 0 \\ 0 & 0 & 1 \end{pmatrix} \quad . \tag{3}$$

Therefore, we find that

$$\mathbf{x}_1 = \mathbf{ABCx} \quad . \tag{4}$$

The equation of an ellipsoid, centered at the origin with its three axes (lengths $2a$, $2b$ and $2c$) located on the $x_1$, $y_1$ and $z_1$ axes, would be

$$(\mathbf{Kx}_1)^T(\mathbf{Kx}_1) = 1 \quad \text{where} \quad \mathbf{K} = \begin{pmatrix} \frac{1}{a} & 0 & 0 \\ 0 & \frac{1}{b} & 0 \\ 0 & 0 & \frac{1}{c} \end{pmatrix} \quad . \tag{5}$$

Using (4), we can rewrite (5) as

$$(\mathbf{KABCx})^T(\mathbf{KABCx}) = 1 \quad . \tag{6}$$

For a spherical polar coordinate system using $r$ (radius), $\theta$ (angle measured from the positive $z$ direction), and $\phi$ (angle measured in the $xy$ plane from the positive $x$ direction), we have

$$\mathbf{x} = r\hat{\mathbf{r}} \quad \text{where} \quad \hat{\mathbf{r}} = \begin{pmatrix} \sin\theta\cos\phi \\ \sin\theta\sin\phi \\ \cos\theta \end{pmatrix} \quad . \tag{7}$$

We can rewrite (6), in spherical polar form, as

$$r^2(\mathbf{V}^T\mathbf{V}) = 1 \quad \text{where} \quad \mathbf{V} = \mathbf{KABC}\hat{\mathbf{r}} \quad . \tag{8}$$

We can solve (8) for $r$ as a function of $\theta$ and $\phi$, thereby describing the surface of the ellipsoid.

### 2.1.1 Ellipsoidal Projection onto the $xy$ Plane

In order to determine the ellipsoidal projection onto a two dimensional plane say the $xy$ plane, consider a cross sectional plane through the center of the ellipsoid and perpendicular to the $xy$ plane. for some arbitrary angle $o$ (where $o$ is measured from the positive $x$ direction in the $xy$ plane to the cross sectional plane).

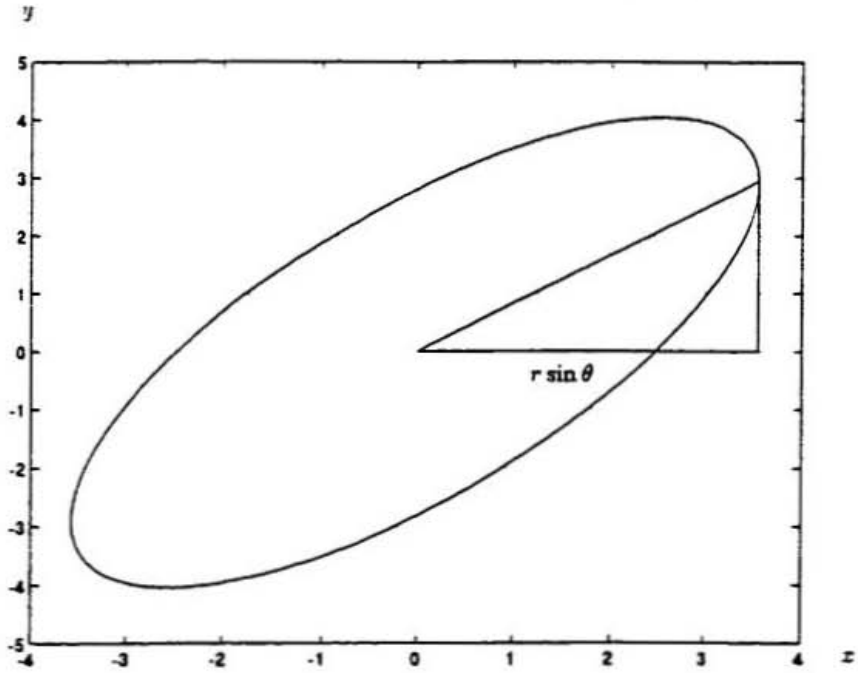


Figure 6: Cross sectional view of the ellipsoid taken perpendicular to the $xy$ plane.

The projection points are found by maximizing $r\sin\theta$ with respect to $\theta$ (Figure 6). That is, we must solve the equation,

$$\frac{\partial}{\partial\theta}(r\sin\theta) = 0 \quad . \tag{9}$$

This will yield the value of $\theta$ (say $\theta_0$) at which $r\sin\theta$ is equal to the distance from the origin to the projection point, in the $xy$ plane. Note that $\theta_0$ will be a function of $\phi$. The

projection points will then be given by

$$\rho_1(\phi) \equiv r(\theta_0(\phi), \phi)\sin(\theta_0(\phi)) \quad . \tag{10}$$

where $\rho_1(\phi)$ is the distance from the origin to the projection point. at angle $\phi$ in the $xy$ plane ($\rho\phi z$ cylindrical coordinate system).

From (9), we have

$$\frac{\partial r}{\partial \theta}\sin\theta + r\cos\theta = 0 \quad . \tag{11}$$

Using (8), we can find an expression for $\frac{\partial r}{\partial \theta}$,

$$\begin{aligned}\frac{\partial r}{\partial \theta} &= \frac{\partial}{\partial \theta}\left(\frac{1}{(\mathbf{V}^T\mathbf{V})^{1/2}}\right) \\ &= \frac{-1}{2(\mathbf{V}^T\mathbf{V})^{3/2}}\left[\frac{\partial(\mathbf{V}^T)}{\partial\theta}\mathbf{V} + \mathbf{V}^T\frac{\partial \mathbf{V}}{\partial\theta}\right] \quad .\end{aligned} \tag{12}$$

For any matrix $\mathbf{M}$, the operations of differentiation and transposition are commutative (i.e. $\frac{\partial(\mathbf{M}^T)}{\partial\theta} = \left(\frac{\partial \mathbf{M}}{\partial\theta}\right)^T$). Also, for any column matrices of the same dimension, say $\mathbf{\Phi}$ and $\mathbf{\Psi}$, we have $\mathbf{\Phi}^T\mathbf{\Psi} = \left(\mathbf{\Phi}^T\mathbf{\Psi}\right)^T$ since $\mathbf{\Phi}^T\mathbf{\Psi}$ is a $1\times 1$ matrix. Therefore, we have the following result,

$$\begin{aligned}\frac{\partial(\mathbf{V}^T)}{\partial\theta}\mathbf{V} &= \left(\frac{\partial \mathbf{V}}{\partial\theta}\right)^T\mathbf{V} \\ &= \left(\left(\frac{\partial \mathbf{V}}{\partial\theta}\right)^T\mathbf{V}\right)^T \\ &= \mathbf{V}^T\frac{\partial \mathbf{V}}{\partial\theta} \quad .\end{aligned} \tag{13}$$

Substituting (8), (12), and (13) into (11), we have after simplifying, the following string of equalities,

$$-\mathbf{V}^T\frac{\partial \mathbf{V}}{\partial\theta}\sin\theta + \mathbf{V}^T\mathbf{V}\cos\theta = 0$$

$$\mathbf{V}^T\left[\mathbf{V}\cos\theta - \frac{\partial \mathbf{V}}{\partial\theta}\sin\theta\right] = 0$$

$$(\mathbf{KABC}\hat{\mathbf{r}})^T\left[\mathbf{KABC}\hat{\mathbf{r}}\cos\theta - \mathbf{KABC}\frac{\partial\hat{\mathbf{r}}}{\partial\theta}\sin\theta\right] = 0$$

$$\hat{\mathbf{r}}^T(\mathbf{KABC})^T(\mathbf{KABC})\left[\hat{\mathbf{r}}\cos\theta - \frac{\partial\hat{\mathbf{r}}}{\partial\theta}\sin\theta\right] = 0$$

$$\hat{\mathbf{r}}^T(\mathbf{KABC})^T(\mathbf{KABC})\begin{pmatrix}0\\0\\1\end{pmatrix} = 0 \quad . \tag{14}$$

where we use the cartesian representation $\hat{\mathbf{r}} = (\sin\theta\cos\phi, \sin\theta\sin\phi, \cos\theta)$.

If we let $\mathbf{\Omega}_1 \equiv (\mathbf{KABC})^T(\mathbf{KABC})$, we have

$$\mathbf{\Omega}_1 = \begin{pmatrix}\omega_{11} & \omega_{12} & \omega_{13}\\ \omega_{21} & \omega_{22} & \omega_{23}\\ \omega_{31} & \omega_{32} & \omega_{33}\end{pmatrix} \quad .$$

where

$$\begin{aligned}
\omega_{11} =& \frac{1}{a^2}\cos^2\beta\cos^2\gamma + \frac{1}{b^2}[\sin\alpha\sin\beta\cos\gamma - \cos\alpha\sin\gamma]^2\\
&+ \frac{1}{c^2}[\cos\alpha\sin\beta\cos\gamma + \sin\alpha\sin\gamma]^2 \quad ,\\
\omega_{12} =& \frac{1}{a^2}\cos^2\beta\cos\gamma\sin\gamma\\
&+ \frac{1}{b^2}[\sin\alpha\sin\beta\sin\gamma + \cos\alpha\cos\gamma][\sin\alpha\sin\beta\cos\gamma - \cos\alpha\sin\gamma]\\
&+ \frac{1}{c^2}[\cos\alpha\sin\beta\cos\gamma + \sin\alpha\sin\gamma][\cos\alpha\sin\beta\sin\gamma - \sin\alpha\cos\gamma] \quad ,\\
\omega_{13} =& -\frac{1}{a^2}\cos\beta\sin\beta\cos\gamma + \frac{1}{b^2}\sin\alpha\cos\beta[\sin\alpha\sin\beta\cos\gamma - \cos\alpha\sin\gamma]\\
&+ \frac{1}{c^2}\cos\alpha\cos\beta[\cos\alpha\sin\beta\cos\gamma + \sin\alpha\sin\gamma] \quad ,\\
\omega_{21} =& \omega_{12} \quad ,\\
\omega_{22} =& \frac{1}{a^2}\cos^2\beta\sin^2\gamma + \frac{1}{b^2}[\sin\alpha\sin\beta\sin\gamma + \cos\alpha\cos\gamma]^2\\
&+ \frac{1}{c^2}[\cos\alpha\sin\beta\sin\gamma - \sin\alpha\cos\gamma]^2 \quad ,\\
\omega_{23} =& -\frac{1}{a^2}\cos\beta\sin\beta\sin\gamma + \frac{1}{b^2}\sin\alpha\cos\beta[\sin\alpha\sin\beta\sin\gamma + \cos\alpha\cos\gamma]
\end{aligned} \tag{15}$$

$$+\frac{1}{c^2}\cos\alpha\cos\beta[\cos\alpha\sin\beta\sin\gamma-\sin\alpha\cos\gamma] \quad .$$

$$\omega_{31}=\omega_{13} \quad ,$$

$$\omega_{32}=\omega_{23} \quad ,$$

$$\omega_{33}=\frac{1}{a^2}\sin^2\beta+\frac{1}{b^2}\sin^2\alpha\cos^2\beta+\frac{1}{c^2}\cos^2\alpha\cos^2\beta \quad .$$

We can now rewrite (8) as,

$$\begin{aligned} r^{-2} &= \mathbf{V}^T\mathbf{V} \\ &= (\mathbf{KABC}\hat{\mathbf{r}})^T(\mathbf{KABC}\hat{\mathbf{r}}) \\ &= \hat{\mathbf{r}}^T\boldsymbol{\Omega}_1\hat{\mathbf{r}} \quad . \end{aligned} \tag{16}$$

Using $\boldsymbol{\Omega}_1 = (\mathbf{KABC})^T(\mathbf{KABC})$, we can rewrite (14) as

$$\hat{\mathbf{r}}^T\boldsymbol{\Omega}_1\begin{pmatrix}0\\0\\1\end{pmatrix}=0 \quad ,$$

$$\text{that is} \qquad \hat{\mathbf{r}}^T\begin{pmatrix}\omega_{13}\\\omega_{23}\\\omega_{33}\end{pmatrix}=0 \quad ,$$

$$\text{or} \qquad \omega_{13}\sin\theta\cos\phi+\omega_{23}\sin\theta\sin\phi+\omega_{33}\cos\theta=0 \quad . \tag{17}$$

From (17), we can find solve for $\sin\theta$ or $\cos\theta$,

$$\begin{aligned} \sin\theta &= \frac{\omega_{33}}{[\omega_{33}^2+(\omega_{13}\cos\phi+\omega_{23}\sin\phi)^2]^{\frac{1}{2}}} \quad , \\ \cos\theta &= \frac{-\omega_{13}\cos\phi-\omega_{23}\sin\phi}{[\omega_{33}^2+(\omega_{13}\cos\phi+\omega_{23}\sin\phi)^2]^{\frac{1}{2}}} \quad . \end{aligned} \tag{18}$$

Note that (18) ensures that $\sin\theta \geq 0$, which must be the case since $0 \leq \theta \leq \pi$. We now effectively have $r$ in terms of $\phi$ (through (16) and (18)) and $\theta$ in terms of $\phi$ (through (18)).

Thus we can rewrite (10) as

$$\rho_1 = \left\{ \frac{1}{\omega_{33}} \left[ \cos^2\phi\,(\omega_{11}\omega_{33} - \omega_{13}\omega_{31}) + \sin^2\phi\,(\omega_{22}\omega_{33} - \omega_{23}\omega_{32}) \right.\right.$$
$$\left.\left. + \cos\phi\sin\phi\,(\omega_{12}\omega_{33} + \omega_{21}\omega_{33} - \omega_{13}\omega_{32} - \omega_{23}\omega_{31}) \right] \right\}^{-\frac{1}{2}} . \qquad (19)$$

If we substitute (15) into (19), we arrive at a cylindrical representation of the ellipsoidal projection,

$$\begin{aligned}
\rho_1 = {} & (b^2c^2\sin^2\beta + a^2c^2\sin^2\alpha\cos^2\beta + a^2b^2\cos^2\alpha\cos^2\beta)^{\frac{1}{2}} \\
& \times \left\{ \cos^2\phi \Big( a^2[\cos^2\beta\sin^2\gamma] + b^2[\sin\alpha\sin\beta\sin\gamma + \cos\alpha\cos\gamma]^2 \right. \\
& \left. + c^2[\cos\alpha\sin\beta\sin\gamma - \sin\alpha\cos\gamma]^2 \Big) \right. \\
& + \sin^2\phi \Big( a^2[\cos^2\beta\cos^2\gamma] + b^2[\sin\alpha\sin\beta\cos\gamma - \cos\alpha\sin\gamma]^2 \Big) \\
& + c^2[\cos\alpha\sin\beta\cos\gamma + \sin\alpha\sin\gamma]^2 \\
& + \cos\phi\sin\phi(2) \Big( -a^2[\cos^2\beta\cos\gamma\sin\gamma] \\
& - b^2[\sin\alpha\sin\beta\sin\gamma + \cos\alpha\cos\gamma][\sin\alpha\sin\beta\cos\gamma - \cos\alpha\sin\gamma] \\
& \left. - c^2[\cos\alpha\sin\beta\cos\gamma + \sin\alpha\sin\gamma][\cos\alpha\sin\beta\sin\gamma - \sin\alpha\cos\gamma] \Big) \right\}^{-\frac{1}{2}} . \qquad (20)
\end{aligned}$$

Recall that $\rho_1$ (cylindrical coordinate parameter) is the distance from the origin to a point on the projection curve of an origin centered ellipsoid projected onto the $xy$ plane. Now we have an equation for $\rho_1$, as a function of the angle $\phi$ measured from the positive $x$ axis. This equation represents the ellipsoidal projection onto the $xy$ plane, in terms of the ellipsoidal axes lengths ($2a$, $2b$, and $2c$) and the original angles of rotation ($\alpha$, $\beta$, and $\gamma$).

The cross section of an ellipsoid has been shown to be an ellipse (Albert, 1949). It is intuitive that the projection of an ellipsoid onto an arbitrary plane can be obtained from

a cross section of the ellipsoid. Thus, the ellipsoidal projection is an ellipse. In order to solve for the ellipsoidal volume, it is necessary to determine a relationship between the ellipsoidal parameters and the ellipse parameters (major axis length, minor axis length, and angle of rotation).

For an ellipse, centered at the origin with its major and minor axes of lengths $2\zeta_1$ and $2\xi_1$ along the $x$ and $y$ axes, respectively, we have

$$(\boldsymbol{\Xi}\mathbf{y})^T(\boldsymbol{\Xi}\mathbf{y}) = 1 \quad \text{where} \quad \boldsymbol{\Xi} = \begin{pmatrix} \frac{1}{\zeta_1} & 0 \\ 0 & \frac{1}{\xi_1} \end{pmatrix} \quad \text{and} \quad \mathbf{y} = \begin{pmatrix} x \\ y \end{pmatrix} \quad . \tag{21}$$

If the ellipse is rotated counter clockwise (Figure 7), say by $\delta_1$ radians, (21) becomes

$$(\boldsymbol{\Xi}\boldsymbol{\Delta}\mathbf{y})^T(\boldsymbol{\Xi}\boldsymbol{\Delta}\mathbf{y}) = 1 \quad \text{where} \quad \boldsymbol{\Delta} = \begin{pmatrix} \cos\delta_1 & \sin\delta_1 \\ -\sin\delta_1 & \cos\delta_1 \end{pmatrix} \quad , \tag{22}$$

which can also be expressed in cylindrical coordinates by

$$\begin{aligned} \rho_1 = \Bigg\{ & \cos^2\phi \left( \frac{\cos^2\delta_1}{\zeta_1^2} + \frac{\sin^2\delta_1}{\xi_1^2} \right) + \sin^2\phi \left( \frac{\cos^2\delta_1}{\xi_1^2} + \frac{\sin^2\delta_1}{\zeta_1^2} \right) \\ & + \cos\phi\sin\phi \left( 2\cos\delta_1 \sin\delta_1 \left[ \frac{1}{\zeta_1^2} - \frac{1}{\xi_1^2} \right] \right) \Bigg\}^{-\frac{1}{2}} \quad . \end{aligned} \tag{23}$$

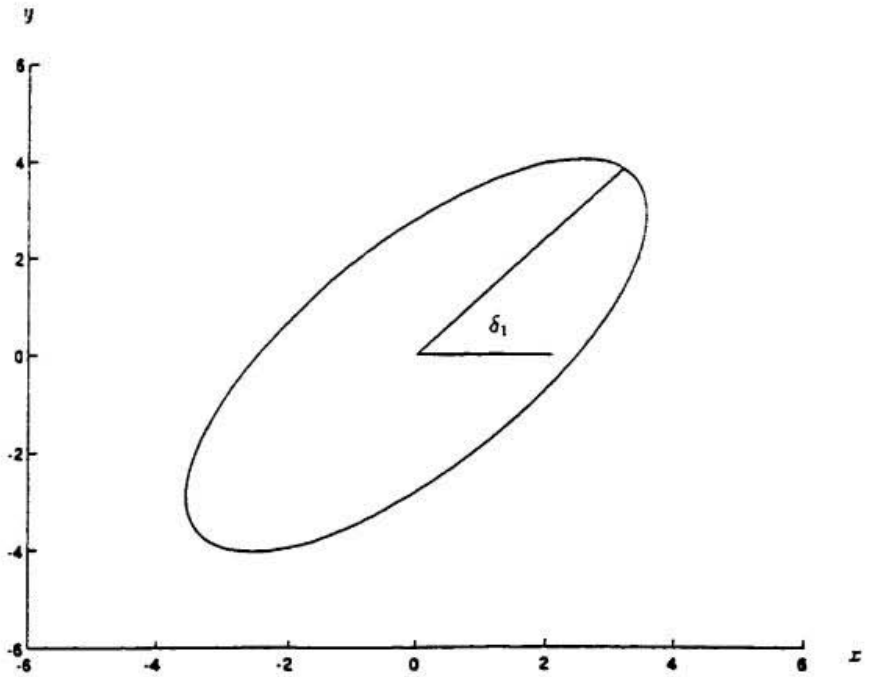


Figure 7: Ellipse in the $xy$ plane, rotated by $\delta_1$ radians.

First of all we shall determine a relationship with $\delta_1$, the angle at which $\rho_1$ is maximum. To find $\delta_1$, we can differentiate (20) with respect to $\phi$ and set it to zero. Let us rewrite (20) as

$$\rho_1 = [\lambda_1 \cos^2\phi + \mu_1 \sin^2\phi + \nu_1 \cos\phi \sin\phi]^{-\frac{1}{2}} \quad , \tag{24}$$

where

$$\begin{aligned}
\lambda_1 = &\left(b^2c^2 \sin^2\beta + a^2c^2 \sin^2\alpha \cos^2\beta + a^2b^2 \cos^2\alpha \cos^2\beta\right)^{-1} \\
&\times \Big(a^2[\cos^2\beta \sin^2\gamma] + b^2[\sin\alpha \sin\beta \sin\gamma + \cos\alpha \cos\gamma]^2 \\
&+ c^2[\cos\alpha \sin\beta \sin\gamma - \sin\alpha \cos\gamma]^2\Big) \quad , \\
\mu_1 = &\left(b^2c^2 \sin^2\beta + a^2c^2 \sin^2\alpha \cos^2\beta + a^2b^2 \cos^2\alpha \cos^2\beta\right)^{-1} \\
&\times \Big(a^2[\cos^2\beta \cos^2\gamma] + b^2[\sin\alpha \sin\beta \cos\gamma - \cos\alpha \sin\gamma]^2 \\
&+ c^2[\cos\alpha \sin\beta \cos\gamma + \sin\alpha \sin\gamma]^2\Big) \quad ,
\end{aligned}$$

$$\nu_1 = \left(b^2c^2\sin^2\beta + a^2c^2\sin^2\alpha\cos^2\beta + a^2b^2\cos^2\alpha\cos^2\beta\right)^{-1}$$

$$\times (2)\Big(-a^2[\cos^2\beta\cos\gamma\sin\gamma]$$

$$- b^2[\sin\alpha\sin\beta\sin\gamma + \cos\alpha\cos\gamma][\sin\alpha\sin\beta\cos\gamma - \cos\alpha\sin\gamma]$$

$$- c^2[\cos\alpha\sin\beta\cos\gamma + \sin\alpha\sin\gamma][\cos\alpha\sin\beta\sin\gamma - \sin\alpha\cos\gamma]\Big) \quad .$$

From (24), we have

$$\frac{\partial\rho_1}{\partial\phi} = -\frac{1}{2}[\lambda_1\cos^2\phi + \mu_1\sin^2\phi + \nu_1\cos\phi\sin\phi]^{-\frac{3}{2}}$$

$$\times [-2\lambda_1\cos\phi\sin\phi + 2\mu_1\cos\phi\sin\phi + \nu_1\cos^2\phi - \nu_1\sin^2\phi] \quad . \tag{25}$$

If we set (25) equal to zero and set $\phi = \delta_1$, we have

$$-2\lambda_1\cos\delta_1\sin\delta_1 + 2\mu_1\cos\delta_1\sin\delta_1 + \nu_1\cos^2\delta_1 - \nu_1\sin^2\delta_1 = 0$$

$$2\cos\delta_1\sin\delta_1[\mu_1 - \lambda_1] = -\nu_1[\cos^2\delta_1 - \sin^2\delta_1]$$

$$\sin(2\delta_1)[\mu_1 - \lambda_1] = -\nu_1\cos(2\delta_1)$$

$$\tan(2\delta_1) = \frac{-\nu_1}{\mu_1 - \lambda_1} \quad . \tag{26}$$

We can then find $\cos(2\delta_1)$ and $\sin(2\delta_1)$ to be

$$\sin(2\delta_1) = \frac{-\nu_1}{[\nu_1^2 + (\mu_1 - \lambda_1)^2]^{\frac{1}{2}}} \quad \text{and} \quad \cos(2\delta_1) = \frac{\mu_1 - \lambda_1}{[\nu_1^2 + (\mu_1 - \lambda_1)^2]^{\frac{1}{2}}} \quad . \tag{27}$$

Using trigonometric identities we also have

$$\cos\delta_1\sin\delta_1 = \frac{-\nu_1}{2[\nu_1^2 + (\mu_1 - \lambda_1)^2]^{\frac{1}{2}}} \quad ,$$

$$\cos^2\delta_1 = \frac{1}{2}\left(1 + \frac{\mu_1 - \lambda_1}{[\nu_1^2 + (\mu_1 - \lambda_1)^2]^{\frac{1}{2}}}\right) \quad ,$$

$$\sin^2\delta_1 = \frac{1}{2}\left(1 - \frac{\mu_1 - \lambda_1}{[\nu_1^2 + (\mu_1 - \lambda_1)^2]^{\frac{1}{2}}}\right) \quad . \tag{28}$$

We can substitute (28) into (24) and simplify to get the following extremum value for $\rho_1$,

$$\rho_1 = \left\{ \frac{1}{2} \left( \lambda_1 + \mu_1 - \left[ \nu_1^2 + (\mu_1 - \lambda_1)^2 \right]^{\frac{1}{2}} \right) \right\}^{-\frac{1}{2}} \quad . \tag{29}$$

To determine another extremum, we should reconsider (26). Strictly speaking, in (26), $\tan(2\delta_1)$ should be $\tan(2\delta_1 + n\pi)$ (where $n$ is an integer) since the tan() function is periodic with period $\pi$. Therefore, we see that another value of $\delta_1$ that will satisfy (26) is $\delta_1 + \pi/2$. If we replace $\delta_1$ with $\delta_1 + \pi/2$, we get

$$\rho_1 = \left\{ \frac{1}{2} \left( \lambda_1 + \mu_1 + \left[ \nu_1^2 + (\mu_1 - \lambda_1)^2 \right]^{\frac{1}{2}} \right) \right\}^{-\frac{1}{2}} \quad . \tag{30}$$

We now see that (29) gives us an expression for the maximum of $\rho_1$ and (30) gives us an expression for the minimum of $\rho_1$.

Let us equate $\zeta_1$ and $\xi_1$ (the half lengths of the major and minor axes) with (29) and (30), respectively, to get

$$\begin{aligned} \zeta_1 &= \left\{ \frac{1}{2} \left( \lambda_1 + \mu_1 - \left[ \nu_1^2 + (\mu_1 - \lambda_1)^2 \right]^{\frac{1}{2}} \right) \right\}^{-\frac{1}{2}} \quad , \\ \xi_1 &= \left\{ \frac{1}{2} \left( \lambda_1 + \mu_1 + \left[ \nu_1^2 + (\mu_1 - \lambda_1)^2 \right]^{\frac{1}{2}} \right) \right\}^{-\frac{1}{2}} \quad . \end{aligned} \tag{31}$$

If we substitute (28) and (31) into (23) and show that the resulting equation is identical to (24), then we will have verified that an ellipsoidal projection is always an ellipse. More importantly, we will have expressions for the major and minor axes lengths, $2\zeta_1$ and $2\xi_1$ respectively, and the angle of rotation ($\delta_1$) for the ellipse.

Let us first consider the $\cos^2\phi$ coefficient in equation (23). From (28) and (31), we

get

$$\frac{\cos^2(\delta_1)}{\zeta_1^2} + \frac{\sin^2(\delta_1)}{\xi_1^2} = \frac{\frac{1}{2}\left(1 + \frac{\mu_1-\lambda_1}{\left[\nu_1^2+(\mu_1-\lambda_1)^2\right]^{\frac{1}{2}}}\right)}{2\left(\lambda_1+\mu_1-\left[\nu_1^2+(\mu_1-\lambda_1)^2\right]^{\frac{1}{2}}\right)^{-1}} + \frac{\frac{1}{2}\left(1 - \frac{\mu_1-\lambda_1}{\left[\nu_1^2+(\mu_1-\lambda_1)^2\right]^{\frac{1}{2}}}\right)}{2\left(\lambda_1+\mu_1+\left[\nu_1^2+(\mu_1-\lambda_1)^2\right]^{\frac{1}{2}}\right)^{-1}}$$

$$= \frac{1}{4}\left(2\lambda_1 - \left[\nu_1^2+(\mu_1-\lambda_1)^2\right]^{\frac{1}{2}} + \frac{\mu_1^2-\lambda_1^2}{\left[\nu_1^2+(\mu_1-\lambda_1)^2\right]^{\frac{1}{2}}}\right)$$

$$+ \frac{1}{4}\left(2\lambda_1 + \left[\nu_1^2+(\mu_1-\lambda_1)^2\right]^{\frac{1}{2}} - \frac{\mu_1^2-\lambda_1^2}{\left[\nu_1^2+(\mu_1-\lambda_1)^2\right]^{\frac{1}{2}}}\right)$$

$$= \lambda_1 \quad . \tag{32}$$

Similarly, we can show that

$$\frac{\cos^2(\delta_1)}{\xi_1^2} + \frac{\sin^2(\delta_1)}{\zeta_1^2} = \mu_1 \quad , \tag{33}$$

and

$$2\cos(\delta_1)\sin(\delta_1)\left(\frac{1}{\zeta_1^2} - \frac{1}{\xi_1^2}\right) = \nu_1 \quad . \tag{34}$$

We can also use (27) to find $\delta_1$ as

$$\delta_1 = \begin{cases} \frac{1}{2}\arccos\left(\frac{\mu_1-\lambda_1}{\left[\nu_1^2+(\mu_1-\lambda_1)^2\right]^{\frac{1}{2}}}\right) & , \quad \text{if } -\nu_1 > 0 \quad ; \\ -\frac{1}{2}\arccos\left(\frac{\mu_1-\lambda_1}{\left[\nu_1^2+(\mu_1-\lambda_1)^2\right]^{\frac{1}{2}}}\right) & , \quad \text{if } -\nu_1 < 0 \quad . \end{cases} \tag{35}$$

Thus, (23) can be rewritten as (24) using (32), (33), and (34). We have now verified that the projection of an ellipsoid onto the $xy$ plane (represented by (24)) can be expressed in a form identical to (23), representing a rotated ellipse in the $xy$ plane. We can thus express the ellipsoidal projection in matrix form as

$$(\boldsymbol{\Xi}\boldsymbol{\Delta}\mathbf{x})^T(\boldsymbol{\Xi}\boldsymbol{\Delta}\mathbf{x}) = 1$$

where $\Xi$ and $\Delta$, originally defined in (21) and (22), are now given by

$$\Xi = \begin{pmatrix} \frac{1}{\sqrt{2}}\left(\lambda_1 + \mu_1 - \left[\nu_1^2 + (\mu_1 - \lambda_1)^2\right]^{\frac{1}{2}}\right)^{\frac{1}{2}} & 0 \\ 0 & \frac{1}{\sqrt{2}}\left(\lambda_1 + \mu_1 + \left[\nu_1^2 + (\mu_1 - \lambda_1)^2\right]^{\frac{1}{2}}\right)^{\frac{1}{2}} \end{pmatrix},$$

$$\Delta = \begin{pmatrix} \frac{1}{\sqrt{2}}\left(1 + \frac{\mu_1 - \lambda_1}{\left[\nu_1^2 + (\mu_1 - \lambda_1)^2\right]^{\frac{1}{2}}}\right)^{\frac{1}{2}} & \frac{1}{\sqrt{2}}\left(1 - \frac{\mu_1 - \lambda_1}{\left[\nu_1^2 + (\mu_1 - \lambda_1)^2\right]^{\frac{1}{2}}}\right)^{\frac{1}{2}} \\ -\frac{1}{\sqrt{2}}\left(1 - \frac{\mu_1 - \lambda_1}{\left[\nu_1^2 + (\mu_1 - \lambda_1)^2\right]^{\frac{1}{2}}}\right)^{\frac{1}{2}} & \frac{1}{\sqrt{2}}\left(1 + \frac{\mu_1 - \lambda_1}{\left[\nu_1^2 + (\mu_1 - \lambda_1)^2\right]^{\frac{1}{2}}}\right)^{\frac{1}{2}} \end{pmatrix}, \quad (36)$$

with $\lambda_1$, $\mu_1$, and $\nu_1$ defined in (24). It should be noted that even though we have found only one projection of this ellipsoid, namely in the $xy$ plane, all other projections can be found by further rotations of the $xyz$ axes such that the new $xy$ plane is parallel to the desired projection plane . This will result in a new matrix $\Omega_1$ which will then give us new expressions for $\lambda_1$, $\mu_1$, and $\nu_1$ in (24). Thus, we have verified that the projection of an ellipsoid, with arbitrary orientation, is always an ellipse and we can find an expression for the equation of this ellipse for every possible planar projection.

For each projection (which is an ellipse) we can write expressions for the major axis length, minor axis length, and the angle of rotation (between the major axis and the horizontal axis of the projection), each as a function of $a$, $b$, $c$, $\alpha$, $\beta$, and $\gamma$ (six unknowns). Note that the major axis length, minor axis length, and the angle of rotation are considered to be *known* values since they can be measured from the projection images. We now have three equations (expressions for $\lambda_1$, $\mu_1$, and $\nu_1$ from (24)) in six unknowns. We need to find another three equations in the same six unknowns in order to have six equations in six unknowns.

### 2.1.2 Ellipsoidal Projection onto the $zy$ Plane

Let us now consider finding the projection onto the $zy$ plane, for the same ellipsoid that was described by (5) with associated angles of $\alpha$, $\beta$, and $\gamma$. If we initially rotated the $xz$ axes about the $y$ axis by $\pi/2$ radians (counter clockwise), then the $x$ axis becomes the $-z$ axis, the $y$ axis remains the $y$ axis, and $z$ axis becomes the $x$ axis. Now the new $xy$ projection is the $zy$ projection in the original coordinate system. One way of performing this axes rotation is to express (4) as

$$\mathbf{x}_2 = \mathbf{ABCD}_2\mathbf{x} \quad , \tag{37}$$

where

$$\mathbf{D}_2 = \begin{pmatrix} 0 & 0 & 1 \\ 0 & 1 & 0 \\ -1 & 0 & 0 \end{pmatrix} \quad .$$

The equation of the ellipsoid becomes

$$(\mathbf{KABCD}_2\mathbf{x})^T(\mathbf{KABCD}_2\mathbf{x}) = 1 \quad . \tag{38}$$

To find the projection of this ellipsoid in the new $xyz$ coordinate system, we can use the previous analysis. Equation (17) would become

$$\hat{\mathbf{r}}^T\mathbf{\Omega}_2 \begin{pmatrix} 0 \\ 0 \\ 1 \end{pmatrix} = 0 \quad , \tag{39}$$

where $\mathbf{\Omega}_2 \equiv (\mathbf{KABCD}_2)^T(\mathbf{KABCD}_2)$. We can express $\mathbf{\Omega}_2$ (containing elements $\omega'_{mn}$) as

$$\mathbf{\Omega}_2 = \begin{pmatrix} \omega'_{11} & \omega'_{12} & \omega'_{13} \\ \omega'_{21} & \omega'_{22} & \omega'_{23} \\ \omega'_{31} & \omega'_{32} & \omega'_{33} \end{pmatrix} = \begin{pmatrix} \omega_{33} & -\omega_{23} & -\omega_{13} \\ -\omega_{23} & \omega_{22} & \omega_{12} \\ -\omega_{13} & \omega_{12} & \omega_{11} \end{pmatrix} \quad , \tag{40}$$

with $\omega_{nm}$ being defined in (15).

The equation of the projection in the new $xy$ plane (which is the original $zy$ plane) would be given as (*cf.* (19))

$$\rho_2 = \left\{ \frac{1}{\omega'_{33}} \left[ \cos^2\phi \left( \omega'_{11}\omega'_{33} - \omega'_{13}\omega'_{31} \right) + \sin^2\phi \left( \omega'_{22}\omega'_{33} - \omega'_{23}\omega'_{32} \right) \right. \right.$$
$$\left. \left. + \cos\phi \sin\phi \left( \omega'_{12}\omega'_{33} + \omega'_{21}\omega'_{33} - \omega'_{13}\omega'_{32} - \omega'_{23}\omega'_{31} \right) \right] \right\}^{-\frac{1}{2}} . \qquad (41)$$

If we substitute (40) into (41) and simplify, we arrive at the following cylindrical representation of the ellipsoidal projection in the $zy$ plane (*cf.* (24)),

$$\rho_2 = \left[ \lambda_2 \cos^2\phi + \mu_2 \sin^2\phi + \nu_2 \cos\phi \sin\phi \right]^{-\frac{1}{2}} , \qquad (42)$$

where

$$\lambda_2 = \left( b^2c^2 \cos^2\beta \cos^2\gamma + a^2c^2 [\sin\alpha \sin\beta \cos\gamma - \cos\alpha \sin\gamma]^2 \right.$$
$$+ a^2b^2 [\cos\alpha \sin\beta \cos\gamma + \sin\alpha \sin\gamma]^2 \Big)^{-1}$$
$$\times \Big( a^2 [\cos^2\beta \sin^2\gamma] + b^2 [\sin\alpha \sin\beta \sin\gamma + \cos\alpha \cos\gamma]^2$$
$$+ c^2 [\cos\alpha \sin\beta \sin\gamma - \sin\alpha \cos\gamma]^2 \Big) ,$$

$$\mu_2 = \left( b^2c^2 \cos^2\beta \cos^2\gamma + a^2c^2 [\sin\alpha \sin\beta \cos\gamma - \cos\alpha \sin\gamma]^2 \right.$$
$$+ a^2b^2 [\cos\alpha \sin\beta \cos\gamma + \sin\alpha \sin\gamma]^2 \Big)^{-1}$$
$$\times \Big( a^2 \sin^2\beta + b^2 \sin^2\alpha \cos^2\beta + c^2 \cos^2\alpha \cos^2\beta \Big) ,$$

$$\nu_2 = \left( b^2c^2 \cos^2\beta \cos^2\gamma + a^2c^2 [\sin\alpha \sin\beta \cos\gamma - \cos\alpha \sin\gamma]^2 \right.$$
$$+ a^2b^2 [\cos\alpha \sin\beta \cos\gamma + \sin\alpha \sin\gamma]^2 \Big)^{-1}$$
$$\times (2) \Big( -a^2 [\cos\beta \sin\beta \sin\gamma + b^2 \sin\alpha \cos\beta [\sin\alpha \sin\beta \sin\gamma + \cos\alpha \cos\gamma]$$
$$+ c^2 \cos\alpha \cos\beta [\cos\alpha \sin\beta \sin\gamma - \sin\alpha \cos\gamma] \Big) .$$

We can now use (31) to express the major ($2\zeta_2$) and minor ($2\xi_2$) axes of this elliptical projection as,

$$\zeta_2 = \left\{ \frac{1}{2} \left( \lambda_2 + \mu_2 - \left[ \nu_2^2 + (\mu_2 - \lambda_2)^2 \right]^{\frac{1}{2}} \right) \right\}^{-\frac{1}{2}} \quad .$$

$$\xi_2 = \left\{ \frac{1}{2} \left( \lambda_2 + \mu_2 + \left[ \nu_2^2 + (\mu_2 - \lambda_2)^2 \right]^{\frac{1}{2}} \right) \right\}^{-\frac{1}{2}} \quad . \tag{43}$$

We also have the angle of rotation (between the major axis and the negative $z$ axis of the orignal $xyz$ coordinate system) expressed as,

$$\delta_2 = \begin{cases} \frac{1}{2} \arccos \left( \frac{\mu_2 - \lambda_2}{\left[ \nu_2^2 + (\mu_2 - \lambda_2)^2 \right]^{\frac{1}{2}}} \right) & , \quad \text{if } -\nu_2 > 0 \quad ; \\ -\frac{1}{2} \arccos \left( \frac{\mu_2 - \lambda_2}{\left[ \nu_2^2 + (\mu_2 - \lambda_2)^2 \right]^{\frac{1}{2}}} \right) & , \quad \text{if } -\nu_2 < 0 \quad . \end{cases} \tag{44}$$

### 2.1.3 Determination of the Ellipsoidal Parameters

Using measurements from both projections, we can write six equations in six unknowns ($\zeta_1$, $\xi_1$, $\delta_1$, $\zeta_2$, $\xi_2$, and $\delta_2$ as functions of $a$, $b$, $c$, $\alpha$, $\beta$, and $\gamma$). In order to solve these equations, some equations have to be multiplied together to obtain simpler equations. It can be shown through simplification that

$$\begin{aligned}\lambda_1\zeta_1^2\xi_1^2 =& a^2[\cos^2\beta\sin^2\gamma] + b^2[\sin\alpha\sin\beta\sin\gamma + \cos\alpha\cos\gamma]^2 \\ &+ c^2[\cos\alpha\sin\beta\sin\gamma - \sin\alpha\cos\gamma]^2\Big) \\ =& \lambda_2\zeta_2^2\xi_2^2 \quad . \end{aligned} \tag{45}$$

This relationship was discovered while trying to solve these six equations in six unknowns. This shows that one of the simplified equations from the first projection plane is the same as one of the simplified equations from the second projection plane. Thus, these six equations are not independent. A unique solution cannot be obtained for $a$, $b$, $c$, $\alpha$, $\beta$, and $\gamma$.

We can also illustrate dependence among these equations by considering the following specific case. Suppose that we have an ellipsoid oriented such that $\alpha = 0$, $\beta = \pi/4$, and $\gamma = 0$. Using definitions for $\lambda_1$, $\mu_1$, and $\nu_1$ from equation (24) along with equations (31) and (35), we can substitute these values of $\alpha$, $\beta$, and $\gamma$ to get the following results. In the $xy$ plane, we have that $\delta_1 = \pi/2$, $\zeta_1 = b$, and $\xi_1 = ([a^2 + c^2]/2)^{1/2}$ if $b > ([a^2 + c^2]/2)^{1/2}$ or $\delta_1 = 0$, $\zeta_1 = ([a^2 + c^2]/2)^{1/2}$, and $\xi_1 = b$ if $b < ([a^2 + c^2]/2)^{1/2}$. Similarly, we can use equations (42), (43), and (44) along with the previous values of $\alpha$, $\beta$, and $\gamma$ to obtain results in the other projection plane. In the $zy$ projection plane, we have $\delta_2 = \delta_1$, $\zeta_2 = \zeta_1$, and $\xi_2 = \xi_1$ (identical to the $xy$ plane projection). Note that it is impossible to solve for $a$

or $c$, individually. If we look along the $y$ axis, we see that a *family* of ellipsoids will result in the identical projection onto the $xy$ and $zy$ planes (Figure 8).

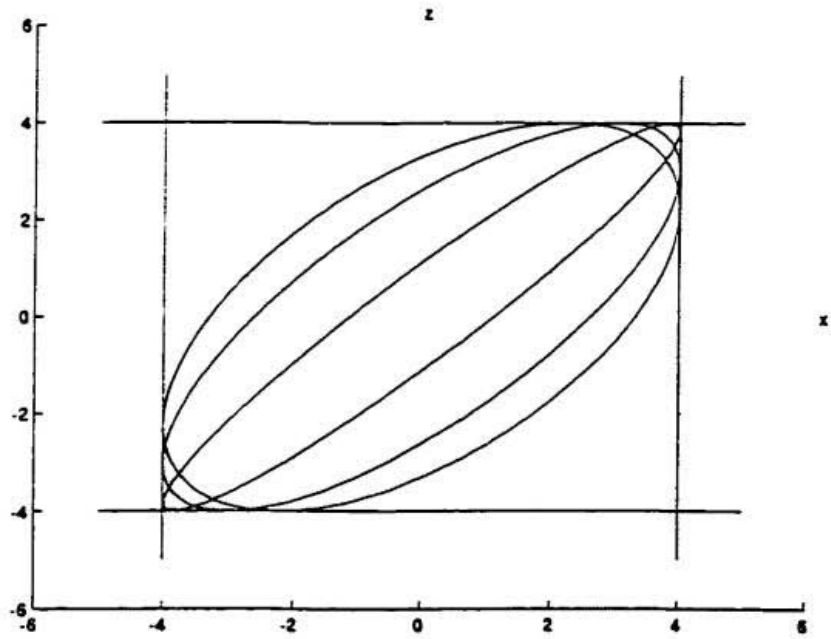


Figure 8: Family of ellipsoids satisfying the special case of $\alpha = 0$, $\beta = \pi/4$, and $\gamma = 0$.

In order to solve for the six unknowns, another equation will be required, from another projection plane. An obvious choice would be to choose the $xz$ projection plane but, practically, it would be difficult to obtain three orthogonal projections of the left ventricle. It is difficult to position the camera in three orthogonal directions without having interference (radiation) from other organs. A more practical choice of the third projection plane is to use the $x = -z$ plane. Thus, if the camera was initially viewing the first projection plane ($xy$ plane), then the camera would have to be rotated 45° to view the third projection plane ($x = -z$ plane) and rotated another 45° (in the same direction as the first 45° rotation) to view the second projection plane ($zy$ plane).

### 2.1.4 Ellipsoidal Projection onto the $x = -z$ Plane

Let us now consider finding the projection onto the $x = -z$ plane, for the same ellipsoid that was arbitrarily situated in $xyz$ space with associated angles of $\alpha$, $\beta$, and $\gamma$. We can perform the necessary axes rotation by expressing (4) as,

$$\mathbf{x}_3 = \mathbf{ABCD}_3\mathbf{x} \quad , \tag{46}$$

where

$$\mathbf{D}_3 = \begin{pmatrix} \frac{1}{\sqrt{2}} & 0 & \frac{1}{\sqrt{2}} \\ 0 & 1 & 0 \\ \frac{-1}{\sqrt{2}} & 0 & \frac{1}{\sqrt{2}} \end{pmatrix} \quad .$$

The equation of the ellipsoid becomes

$$(\mathbf{KABCD}_3\mathbf{x})^T(\mathbf{KABCD}_3\mathbf{x}) = 1 \quad . \tag{47}$$

To find the projection of this ellipsoid in the new $xyz$ coordinate system, we can use the previous analysis. Equation (17) would become,

$$\hat{\mathbf{r}}^T\mathbf{\Omega}_3 \begin{pmatrix} 0 \\ 0 \\ 1 \end{pmatrix} = 0 \quad , \tag{48}$$

where $\mathbf{\Omega}_3 \equiv (\mathbf{KABCD}_3)^T(\mathbf{KABCD}_3)$. We can express $\mathbf{\Omega}_3$ as

$$\mathbf{\Omega}_3 = \begin{pmatrix} \omega''_{11} & \omega''_{12} & \omega''_{13} \\ \omega''_{21} & \omega''_{22} & \omega''_{23} \\ \omega''_{31} & \omega''_{32} & \omega''_{33} \end{pmatrix}$$

where

$$\omega''_{11} = \frac{1}{2a^2}(\cos\beta\cos\gamma + \sin\beta)^2 + \frac{1}{2b^2}(\sin\alpha\sin\beta\cos\gamma - \cos\alpha\sin\gamma - \sin\alpha\cos\beta)^2 + \frac{1}{2c^2}(\cos\alpha\sin\beta\cos\gamma + \sin\alpha\sin\gamma - \cos\alpha\cos\beta)^2 \quad ,$$

$$\omega''_{12} = \frac{1}{\sqrt{2}a^2}\cos\beta\sin\gamma\,(\cos\beta\cos\gamma+\sin\beta)$$
$$+\frac{1}{\sqrt{2}b^2}(\sin\alpha\sin\beta\sin\gamma+\cos\alpha\cos\gamma)(\sin\alpha\sin\beta\cos\gamma-\cos\alpha\sin\gamma-\sin\alpha\cos\beta)$$
$$+\frac{1}{\sqrt{2}c^2}(\cos\alpha\sin\beta\sin\gamma-\sin\alpha\cos\gamma)(\cos\alpha\sin\beta\cos\gamma+\sin\alpha\sin\gamma-\cos\alpha\cos\beta)\quad,$$

$$\omega''_{13} = \frac{1}{2a^2}(\cos^2\beta\cos^2\gamma-\sin^2\beta)+\frac{1}{2b^2}([\sin\alpha\sin\beta\cos\gamma-\cos\alpha\sin\gamma]^2-\sin^2\alpha\cos^2\beta)$$
$$+\frac{1}{2c^2}([\cos\alpha\sin\beta\cos\gamma+\sin\alpha\sin\gamma]^2-\cos^2\alpha\cos^2\beta)\quad,$$

$$\omega''_{21} = \omega''_{12}\quad,$$

$$\omega''_{22} = \frac{1}{a^2}\cos^2\beta\sin^2\gamma+\frac{1}{b^2}[\sin\alpha\sin\beta\sin\gamma+\cos\alpha\cos\gamma]^2$$
$$+\frac{1}{c^2}[\cos\alpha\sin\beta\sin\gamma-\sin\alpha\cos\gamma]^2\quad,\qquad(49)$$

$$\omega''_{23} = \frac{1}{\sqrt{2}a^2}\cos\beta\sin\gamma\,(\cos\beta\cos\gamma-\sin\beta)$$
$$+\frac{1}{\sqrt{2}b^2}(\sin\alpha\sin\beta\sin\gamma+\cos\alpha\cos\gamma)(\sin\alpha\sin\beta\cos\gamma-\cos\alpha\sin\gamma+\sin\alpha\cos\beta)$$
$$+\frac{1}{\sqrt{2}c^2}(\cos\alpha\sin\beta\sin\gamma-\sin\alpha\cos\gamma)(\cos\alpha\sin\beta\cos\gamma+\sin\alpha\sin\gamma+\cos\alpha\cos\beta)\quad,$$

$$\omega''_{31} = \omega''_{13}\quad,$$

$$\omega''_{32} = \omega''_{23}\quad,$$

$$\omega''_{33} = \frac{1}{2a^2}(\cos\beta\cos\gamma-\sin\beta)^2+\frac{1}{2b^2}(\sin\alpha\sin\beta\cos\gamma-\cos\alpha\sin\gamma+\sin\alpha\cos\beta)^2$$
$$+\frac{1}{2c^2}(\cos\alpha\sin\beta\cos\gamma+\sin\alpha\sin\gamma+\cos\alpha\cos\beta)^2\quad.$$

The equation of the projection in the new $xy$ plane (which is the original $x=-z$ plane) would now be given by (*cf.* (19)),

$$\rho_3 = \left\{\frac{1}{\omega''_{33}}\left[\cos^2\phi\,(\omega''_{11}\omega''_{33}-\omega''_{13}\omega''_{31})+\sin^2\phi\,(\omega''_{22}\omega''_{33}-\omega''_{23}\omega''_{32})\right.\right.$$
$$\left.\left.+\cos\phi\sin\phi\,(\omega''_{12}\omega''_{33}+\omega''_{21}\omega''_{33}-\omega''_{13}\omega''_{32}-\omega''_{23}\omega''_{31})\right]\right\}^{-\frac{1}{2}}\quad.\qquad(50)$$

If we substitute (49) into (50) and simplify, we arrive at the following cylindrical representation of the ellipsoidal projection onto the $x = -z$ plane (*cf.* (24)).

$$\rho_3 = [\lambda_3 \cos^2 o + \mu_3 \sin^2 o + \nu_3 \cos o \sin o]^{-\frac{1}{2}} \quad , \tag{51}$$

where

$$\begin{aligned}
\lambda_3 =& 2\big(b^2c^2[\cos\beta\cos\gamma - \sin\beta]^2 + a^2c^2[\sin\alpha\sin\beta\cos\gamma - \cos\alpha\sin\gamma + \sin\alpha\cos\beta]^2 \\
&+ a^2b^2[\cos\alpha\sin\beta\cos\gamma + \sin\alpha\sin\gamma + \cos\alpha\cos\beta]^2\big)^{-1} \\
&\times \Big(a^2[\cos^2\beta\sin^2\gamma] + b^2[\sin\alpha\sin\beta\sin\gamma + \cos\alpha\cos\gamma]^2 \\
&+ c^2[\cos\alpha\sin\beta\sin\gamma - \sin\alpha\cos\gamma]^2\Big) \quad , \\
\mu_3 =& \big(b^2c^2[\cos\beta\cos\gamma - \sin\beta]^2 + a^2c^2[\sin\alpha\sin\beta\cos\gamma - \cos\alpha\sin\gamma + \sin\alpha\cos\beta]^2 \\
&+ a^2b^2[\cos\alpha\sin\beta\cos\gamma + \sin\alpha\sin\gamma + \cos\alpha\cos\beta]^2\big)^{-1} \\
&\times \Big(a^2[\cos\beta\cos\gamma + \sin\beta]^2 + b^2[\sin\alpha\sin\beta\cos\gamma - \cos\alpha\sin\gamma - \sin\alpha\cos\beta]^2 \\
&+ c^2[\cos\alpha\sin\beta\cos\gamma + \sin\alpha\sin\gamma - \cos\alpha\cos\beta]^2\Big) \quad , \\
\nu_3 =& 2\sqrt{2}\big(b^2c^2[\cos\beta\cos\gamma - \sin\beta]^2 + a^2c^2[\sin\alpha\sin\beta\cos\gamma - \cos\alpha\sin\gamma + \sin\alpha\cos\beta]^2 \\
&+ a^2b^2[\cos\alpha\sin\beta\cos\gamma + \sin\alpha\sin\gamma + \cos\alpha\cos\beta]^2\big)^{-1} \\
&\times \Big(-a^2\cos\beta\sin\gamma[\sin\beta + \cos\beta\cos\gamma] \\
&- b^2[\sin\alpha\sin\beta\sin\gamma + \cos\alpha\cos\gamma][\sin\alpha\sin\beta\cos\gamma - \cos\alpha\sin\gamma - \sin\alpha\cos\beta] \\
&- c^2[\cos\alpha\sin\beta\sin\gamma - \sin\alpha\cos\gamma][\cos\alpha\sin\beta\cos\gamma + \sin\alpha\sin\gamma - \cos\alpha\cos\beta]\Big) \quad .
\end{aligned}$$

We can now use (31) to express the major ($2\zeta_3$) and minor ($2\xi_3$) axes of this elliptical projection as,

$$\zeta_3 = \left\{\frac{1}{2}\left(\lambda_3 + \mu_3 - \left[\nu_3^2 + (\mu_3 - \lambda_3)^2\right]^{\frac{1}{2}}\right)\right\}^{-\frac{1}{2}} \quad ,$$

$$\xi_3 = \left\{ \frac{1}{2} \left( \lambda_3 + \mu_3 + \left[ \nu_3^2 + (\mu_3 - \lambda_3)^2 \right]^{\frac{1}{2}} \right) \right\}^{-\frac{1}{2}} \quad . \tag{52}$$

We also have the angle of rotation (between the major axis and the horizontal axis of the camera image ) expressed as,

$$\delta_3 = \begin{cases} \frac{1}{2} \arccos \left( \frac{\mu_3 - \lambda_3}{\left[ \nu_3^2 + (\mu_3 - \lambda_3)^2 \right]^{\frac{1}{2}}} \right) & , \quad \text{if } -\nu_3 > 0 \quad : \\ -\frac{1}{2} \arccos \left( \frac{\mu_3 - \lambda_3}{\left[ \nu_3^2 + (\mu_3 - \lambda_3)^2 \right]^{\frac{1}{2}}} \right) & , \quad \text{if } -\nu_3 < 0 \quad . \end{cases} \tag{53}$$

### 2.1.5 Determination of the Volume of the Ellipsoidal Model

From the three projections, we have nine equations in six unknowns. We shall see that only six of these equations are independent. Instead of expressing these equations using $\zeta_n$, $\xi_n$, and $\delta_n$ directly, it is much simpler to express them using $\lambda_n$, $\mu_n$, and $\nu_n$, where these parameters are defined in (24), (42), and (51). Note that $\lambda_n$, $\mu_n$, and $\nu_n$ are functions of $\zeta_n$, $\xi_n$, and $\delta_n$, which are measured values from each projection. To further simplify these equations, note that,

$$\zeta_n^2\xi_n^2 = \left(\lambda_n\mu_n - \frac{1}{4}\nu_n^2\right)^{-1} \quad , \tag{54}$$

which gives us,

$$\begin{aligned}
\zeta_1^2\xi_1^2 =& (b^2c^2\sin^2\beta + a^2c^2\sin^2\alpha\cos^2\beta + a^2b^2\cos^2\alpha\cos^2\beta) \quad , \\
\zeta_2^2\xi_2^2 =& (b^2c^2\cos^2\beta\cos^2\gamma + a^2c^2[\sin\alpha\sin\beta\cos\gamma - \cos\alpha\sin\gamma]^2 \\
& + a^2b^2[\cos\alpha\sin\beta\cos\gamma + \sin\alpha\sin\gamma]^2) \quad , \\
\zeta_3^2\xi_3^2 =& \frac{1}{2}(b^2c^2[\cos\beta\cos\gamma - \sin\beta]^2 + a^2c^2[\sin\alpha\sin\beta\cos\gamma - \cos\alpha\sin\gamma + \sin\alpha\cos\beta]^2 \\
& + a^2b^2[\cos\alpha\sin\beta\cos\gamma + \sin\alpha\sin\gamma + \cos\alpha\cos\beta]^2) \quad .
\end{aligned} \tag{55}$$

We can now simplify (eliminate the denominator terms in) our nine equations (given within (24), (42), and (51)) by expressing them as $\lambda_n\zeta_n^2\xi_n^2$, $\mu_n\zeta_n^2\xi_n^2$, and $\nu_n\zeta_n^2\xi_n^2$. We thus have,

$$\begin{aligned}
\lambda_1\zeta_1^2\xi_1^2 =& a^2[\cos^2\beta\sin^2\gamma] + b^2[\sin\alpha\sin\beta\sin\gamma + \cos\alpha\cos\gamma]^2 \\
& + c^2[\cos\alpha\sin\beta\sin\gamma - \sin\alpha\cos\gamma]^2 \quad ,
\end{aligned}$$

$$\mu_1\zeta_1^2\xi_1^2 = a^2[\cos^2 \beta \cos^2 \gamma] + b^2[\sin\alpha \sin\beta \cos\gamma - \cos\alpha \sin\gamma]^2$$
$$+ c^2[\cos\alpha \sin\beta \cos\gamma + \sin\alpha \sin\gamma]^2 \quad ,$$

$$\nu_1\zeta_1^2\xi_1^2 = 2(-a^2[\cos^2 \beta \cos\gamma \sin\gamma]$$
$$- b^2[\sin\alpha \sin\beta \sin\gamma + \cos\alpha \cos\gamma][\sin\alpha \sin\beta \cos\gamma - \cos\alpha \sin\gamma]$$
$$- c^2[\cos\alpha \sin\beta \cos\gamma + \sin\alpha \sin\gamma][\cos\alpha \sin\beta \sin\gamma - \sin\alpha \cos\gamma]) \quad .$$

$$\lambda_2\zeta_2^2\xi_2^2 = a^2[\cos^2 \beta \sin^2 \gamma] + b^2[\sin\alpha \sin\beta \sin\gamma + \cos\alpha \cos\gamma]^2$$
$$+ c^2[\cos\alpha \sin\beta \sin\gamma - \sin\alpha \cos\gamma]^2 \quad ,$$

$$\mu_2\zeta_2^2\xi_2^2 = a^2 \sin^2 \beta + b^2 \sin^2\alpha \cos^2 \beta + c^2 \cos^2\alpha \cos^2 \beta \quad , \qquad (56)$$

$$\nu_2\zeta_2^2\xi_2^2 = 2(-a^2[\cos\beta \sin\beta \sin\gamma] + b^2 \sin\alpha \cos\beta[\sin\alpha \sin\beta \sin\gamma + \cos\alpha \cos\gamma]$$
$$+ c^2 \cos\alpha \cos\beta[\cos\alpha \sin\beta \sin\gamma - \sin\alpha \cos\gamma]) \quad ,$$

$$\lambda_3\zeta_3^2\xi_3^2 = a^2[\cos^2 \beta \sin^2 \gamma] + b^2[\sin\alpha \sin\beta \sin\gamma + \cos\alpha \cos\gamma]^2$$
$$+ c^2[\cos\alpha \sin\beta \sin\gamma - \sin\alpha \cos\gamma]^2 \quad ,$$

$$\mu_3\zeta_3^2\xi_3^2 = \frac{1}{2}(a^2[\cos\beta \cos\gamma + \sin\beta]^2 + b^2[\sin\alpha \sin\beta \cos\gamma - \cos\alpha \sin\gamma - \sin\alpha \cos\beta]^2$$
$$+ c^2[\cos\alpha \sin\beta \cos\gamma + \sin\alpha \sin\gamma - \cos\alpha \cos\beta]^2) \quad ,$$

$$\nu_3\zeta_3^2\xi_3^2 = \sqrt{2}(-a^2 \cos\beta \sin\gamma[\sin\beta + \cos\beta \cos\gamma]$$
$$- b^2[\sin\alpha \sin\beta \sin\gamma + \cos\alpha \cos\gamma][\sin\alpha \sin\beta \cos\gamma - \cos\alpha \sin\gamma - \sin\alpha \cos\beta]$$
$$- c^2[\cos\alpha \sin\beta \sin\gamma - \sin\alpha \cos\gamma][\cos\alpha \sin\beta \cos\gamma + \sin\alpha \sin\gamma - \cos\alpha \cos\beta]) \quad .$$

Note that we have the following relations,

$$\lambda_1\zeta_1^2\xi_1^2 = \lambda_2\zeta_2^2\xi_2^2 \quad ,$$
$$\lambda_1\zeta_1^2\xi_1^2 = \lambda_3\zeta_3^2\xi_3^2 \quad , \qquad (57)$$

$$\nu_3\zeta_3^2\xi_3^2 = \frac{1}{\sqrt{2}}\left(\nu_1\zeta_1^2\xi_1^2 + \nu_2\zeta_2^2\xi_2^2\right) \quad .$$

This allows us to reduce our set of nine equations to six independent equations. in six unknowns. To help simplify the analysis. we shall also use the equations defined in (54) with our six remaining equations. Note that we are not adding extra independent equations to our equation set since the equations in (54) are functions of $\lambda_n$, $\mu_n$, and $\nu_n$. Thus, the task is now to solve the following equations for $a$, $b$, and $c$.

$$\begin{aligned}
\tau_1 \equiv & \lambda_1\zeta_1^2\xi_1^2 = a^2[\cos^2\beta\sin^2\gamma] + b^2[\sin\alpha\sin\beta\sin\gamma + \cos\alpha\cos\gamma]^2 \\
& + c^2[\cos\alpha\sin\beta\sin\gamma - \sin\alpha\cos\gamma]^2 \quad , \\
\tau_2 \equiv & \mu_1\zeta_1^2\xi_1^2 = a^2[\cos^2\beta\cos^2\gamma] + b^2[\sin\alpha\sin\beta\cos\gamma - \cos\alpha\sin\gamma]^2 \\
& + c^2[\cos\alpha\sin\beta\cos\gamma + \sin\alpha\sin\gamma]^2 \quad , \\
\tau_3 \equiv & \nu_1\zeta_1^2\xi_1^2 = 2\big(-a^2[\cos^2\beta\cos\gamma\sin\gamma] \\
& - b^2[\sin\alpha\sin\beta\sin\gamma + \cos\alpha\cos\gamma][\sin\alpha\sin\beta\cos\gamma - \cos\alpha\sin\gamma] \\
& - c^2[\cos\alpha\sin\beta\cos\gamma + \sin\alpha\sin\gamma][\cos\alpha\sin\beta\sin\gamma - \sin\alpha\cos\gamma]\big) \quad , \\
\tau_4 \equiv & \zeta_1^2\xi_1^2 = \left(b^2c^2\sin^2\beta + a^2c^2\sin^2\alpha\cos^2\beta + a^2b^2\cos^2\alpha\cos^2\beta\right) \quad , \\
\tau_5 \equiv & \mu_2\zeta_2^2\xi_2^2 = a^2\sin^2\beta + b^2\sin^2\alpha\cos^2\beta + c^2\cos^2\alpha\cos^2\beta \quad , \qquad (58) \\
\tau_6 \equiv & \nu_2\zeta_2^2\xi_2^2 = 2\big(-a^2[\cos\beta\sin\beta\sin\gamma + b^2\sin\alpha\cos\beta[\sin\alpha\sin\beta\sin\gamma + \cos\alpha\cos\gamma] \\
& + c^2\cos\alpha\cos\beta[\cos\alpha\sin\beta\sin\gamma - \sin\alpha\cos\gamma]\big) \quad , \\
\tau_7 \equiv & \zeta_2^2\xi_2^2 = \left(b^2c^2\cos^2\beta\cos^2\gamma + a^2c^2[\sin\alpha\sin\beta\cos\gamma - \cos\alpha\sin\gamma]^2\right. \\
& \left. + a^2b^2[\cos\alpha\sin\beta\cos\gamma + \sin\alpha\sin\gamma]^2\right) \quad , \\
\tau_8 \equiv & \mu_3\zeta_3^2\xi_3^2 = \frac{1}{2}\left(a^2[\cos\beta\cos\gamma + \sin\beta]^2 + b^2[\sin\alpha\sin\beta\cos\gamma - \cos\alpha\sin\gamma - \sin\alpha\cos\beta]^2\right.
\end{aligned}$$

$$+ c^2[\cos\alpha \sin\beta \cos\gamma + \sin\alpha \sin\gamma - \cos\alpha \cos\beta]^2) \quad ,$$

$$\tau_9 \equiv \zeta_3^2 \xi_3^2 = \frac{1}{2}(b^2c^2[\cos\beta \cos\gamma - \sin\beta]^2 + a^2c^2[\sin\alpha \sin\beta \cos\gamma - \cos\alpha \sin\gamma + \sin\alpha \cos\beta]^2$$

$$+ a^2b^2[\cos\alpha \sin\beta \cos\gamma + \sin\alpha \sin\gamma + \cos\alpha \cos\beta]^2) \quad .$$

Since only the ellipsoid axes lengths are needed to calculate the volume, we must first eliminate the unknowns $\alpha$, $\beta$, and $\gamma$ from our equation set. With the use of trigonometric identities, it can be shown that,

$$\begin{aligned} \kappa_1 \equiv & \tau_1 + \tau_2 + \tau_5 \\ = & a^2 + b^2 + c^2 \quad . \end{aligned} \tag{59}$$

It can also be shown that,

$$\begin{aligned} \kappa_2 \equiv & \tau_5(\tau_1 + \tau_2) - \frac{1}{4}(2\tau_8 - \tau_5 - \tau_2)^2 + \tau_4 - \frac{1}{4}\tau_6^2 \\ = & b^2c^2 + a^2c^2 + a^2b^2 \quad . \end{aligned} \tag{60}$$

We now need one more equation involving the variables $a$, $b$, and $c$. Consider

$$\begin{aligned} \kappa_3 \equiv & \frac{1}{2}(2\tau_9 - \tau_4 - \tau_7) \\ = & -b^2c^2[\cos\beta \sin\beta \cos\gamma] + a^2c^2(\sin\alpha \cos\beta[\sin\alpha \sin\beta \cos\gamma - \cos\alpha \sin\gamma) \\ & + a^2b^2(\cos\alpha \cos\beta[\cos\alpha \sin\beta \cos\gamma + \sin\alpha \sin\gamma]) \quad . \end{aligned} \tag{61}$$

It can then be shown that,

$$\begin{aligned} \kappa_4 \equiv & \tau_8 - \frac{1}{2}(\tau_2 + \tau_5) \\ = & a^2[\cos\beta \sin\beta \cos\gamma] - b^2(\sin\alpha \cos\beta[\sin\alpha \sin\beta \cos\gamma - \cos\alpha \sin\gamma) \\ & - c^2(\cos\alpha \cos\beta[\cos\alpha \sin\beta \cos\gamma + \sin\alpha \sin\gamma]) \quad . \end{aligned} \tag{62}$$

We can use (61) and (62) to show that,

$$(a^2\kappa_4 - \kappa_3)^2 = (a^2 - b^2)^2(a^2 - c^2)^2 \cos^2 \beta \sin^2 \beta \cos^2 \gamma \quad . \tag{63}$$

We now need expressions for $\cos^2 \beta$, $\sin^2 \beta$, and $\cos^2 \gamma$ in terms of $a$, $b$, $c$, and known values. An expression for $\sin^2 \beta$ can be found using similarities found in the equations of (58):

$$\begin{aligned} \tau_4 - a^2(\tau_1 + \tau_2) &= (a^2 - b^2)(a^2 - c^2)\sin^2 \beta - a^4 \\ \sin^2 \beta &= \frac{a^4 - a^2(\tau_1 + \tau_2) + \tau_4}{(a^2 - b^2)(a^2 - c^2)} \quad . \end{aligned} \tag{64}$$

We can use $\cos^2 \beta = 1 - \sin^2 \beta$ to find an expression for $\cos^2 \beta$ as,

$$\cos^2 \beta = \frac{(a^2 - b^2)(a^2 - c^2) - [a^4 - a^2(\tau_1 + \tau_2) + \tau_4]}{(a^2 - b^2)(a^2 - c^2)} \quad . \tag{65}$$

We can also use $\tau_1$, $\tau_2$, and $\tau_4$ to show that,

$$\sin^2 \alpha = \frac{-(a^2 - c^2)[b^4 - b^2(\tau_1 + \tau_2) + \tau_4]}{(b^2 - c^2)\{(a^2 - b^2)(a^2 - c^2) - [a^4 - a^2(\tau_1 + \tau_2) + \tau_4]\}} \quad , \tag{66}$$

and

$$\cos^2 \alpha = \frac{(a^2 - b^2)[c^4 - c^2(\tau_1 + \tau_2) + \tau_4]}{(b^2 - c^2)\{(a^2 - b^2)(a^2 - c^2) - [a^4 - a^2(\tau_1 + \tau_2) + \tau_4]\}} \quad . \tag{67}$$

The previous four equations can then be used to show that,

$$\sin^2 \gamma = \frac{a^2\tau_1 + b^2c^2 - \tau_4 - \tau_7}{(a^2 - b^2)(a^2 - c^2) - [a^4 - a^2(\tau_1 + \tau_2) + \tau_4]} \quad , \tag{68}$$

and

$$\cos^2 \gamma = \frac{a^2\tau_2 - a^2b^2 - a^2c^2 + \tau_7}{(a^2 - b^2)(a^2 - c^2) - [a^4 - a^2(\tau_1 + \tau_2) + \tau_4]} \quad . \tag{69}$$

We can now substitute (64), (65), and (69) into (63), and simplify to get

$$(a^2\kappa_4 - \kappa_3)^2 = [a^4 - a^2(\tau_1 + \tau_2) + \tau_4][a^2\tau_2 - a^2b^2 - a^2c^2 + \tau_7] \quad . \tag{70}$$

This equation can be expanded and expressed as a quartic in $a^2$ using (59).

$$\begin{aligned} &a^8 + a^6(\tau_1 - \kappa_1) + a^4(\tau_7 - \kappa_4^2 - \tau_1\tau_2 + \tau_1\kappa_1 - \tau_2^2 + \tau_2\kappa_1 + \tau_4) \\ &+ a^2(2\kappa_3\kappa_4 - \tau_1\tau_7 - \tau_2\tau_7 + \tau_2\tau_4 - \tau_4\kappa_1) + \tau_4\tau_7 - \kappa_3^2 = 0 \quad . \end{aligned} \tag{71}$$

Using (54) and (57), it can be shown that

$$\begin{aligned} \tau_4 &= \tau_1\tau_2 - \frac{1}{4}\tau_3^2 \quad , \\ \tau_7 &= \tau_1\tau_5 - \frac{1}{4}\tau_6^2 \quad , \\ \tau_9 &= \tau_1\tau_8 - \frac{1}{4}\left(\frac{1}{2}\tau_3^2 + \tau_3\tau_6 + \frac{1}{2}\tau_6^2\right) \quad . \end{aligned} \tag{72}$$

We can now re-express $\kappa_3$ in (61) as

$$\begin{aligned} \kappa_3 &\equiv \frac{1}{2}(2\tau_9 - \tau_4 - \tau_7) \\ &= \tau_1\tau_8 - \frac{1}{2}\tau_1\tau_2 - \frac{1}{2}\tau_1\tau_5 - \frac{1}{4}\tau_3\tau_6 \\ &= \tau_1\kappa_4 - \frac{1}{4}\tau_3\tau_6 \quad . \end{aligned} \tag{73}$$

If we use (59) and (73) to substitute for $\kappa_1$ and $\kappa_3$ in (71), we have,

$$\begin{aligned} &a^8 + a^6(-2\tau_1 - \tau_2 - \tau_5) + a^4(\tau_7 - \kappa_4^2 + \tau_1^2 + \tau_1\tau_2 + \tau_1\tau_5 + \tau_2\tau_5 + \tau_4) \\ &+ a^2(2\tau_1\kappa_4^2 - \frac{1}{2}\tau_3\tau_6\kappa_4 - \tau_1\tau_7 - \tau - 2\tau_7 - \tau_1\tau_4 - \tau_4\tau_5) \\ &+ \tau_4\tau_7 - \tau_1^2\kappa_4^2 + \frac{1}{2}\tau_1\tau_3\tau_6\kappa_4 - \frac{1}{16}\tau_3^2\tau_6^2 = 0 \quad . \end{aligned} \tag{74}$$

Using (72) we have

$$\tau_4\tau_7 = \tau_1^2\tau_2\tau_5 - \frac{1}{4}\tau_1\tau_2\tau_6^2 - \frac{1}{4}\tau_1\tau_5\tau_3^2 + \frac{1}{16}\tau_3^2\tau_6^2 \quad . \tag{75}$$

If we substitute (75) into (74) and factor, we arrive at,

$$(a^2 - \tau_1)\left(a^6 + a^4[-\kappa_1] + a^2\kappa_2 + \kappa_5\right) = 0 \quad . \tag{76}$$

where

$$\kappa_5 \equiv \tau_1\tau_2\tau_5 - \tau_2\tau_7 - \tau_4\tau_5 + \tau_1\kappa_4^2 - \frac{1}{2}\tau_3\tau_6\kappa_4 \quad .$$

In general, $a^2$ will not always be equal to $\tau_1$, thus,

$$a^6 + a^4[-\kappa_1] + a^2\kappa_2 + \kappa_5 = 0 \quad . \tag{77}$$

It turns out that the three roots of this cubic equation in $a^2$ yield the quantities of $a^2$, $b^2$, and $c^2$ where $a$, $b$, and $c$ are the semi-axes lengths of the ellipsoid. It is impossible to determine which is $a^2$, $b^2$, or $c^2$ since we arbitrarily placed $2a$ along the $x$ axis, $2b$ along the $y$ axis, and $2c$ along the $z$ axis in the original ellipsoid.

With the use of (59) and (60), it can also be shown that (77) can be expressed as,

$$a^2b^2c^2 + \kappa_5 = 0$$

$$\text{whence} \qquad a^2b^2c^2 = -\kappa_5 \quad . \tag{78}$$

Since the volume of an ellipsoid is given as $\frac{4}{3}\pi abc$, we can now estimate the volume of the left ventricle using (78). Note that $\kappa_5$ can be written in terms of measurable quantities $\zeta_n$, $\xi_n$, and $\delta_n$, through the use of (76), (58), and the generalized versions of (32), (33), and (34).

# Chapter 3:
# Results and Discussion

To test the accuracy of using this ellisoidal model for left ventricular volume estimation, two identical hollow ellipsoidal models were constructed. The inner dimensions of each axis ($9.2cm$, $5.8cm$, and $3.6cm$) were chosen so that the axes ratios would be similar to those found in a left ventricle. A $^{99m}Tc$ solution was injected into the models which were then placed under a gamma ($\gamma$) camera.

Counts were recorded for a period of two minutes to ensure a relatively clear image of each model (Figure 9). The camera was then rotated 45° and a new image was recorded. Finally, the camera was rotated another 45° along the same arc as the first rotation to obtain an image in the third viewing direction. A total of 20 trials (10 trials with two models imaged in each trial) were performed in which the models were arbitrarily located relative to a fixed reference frame. Trials 1 and 2 were performed on separate occasions using a different concentration of radionuclide, thus causing a different number of counts. Also, the odd numbered trials between 3 and 19 (inclusive) were performed with one model while the even numbered trials between 4 and 20 (inclusive) were performed with the other model.

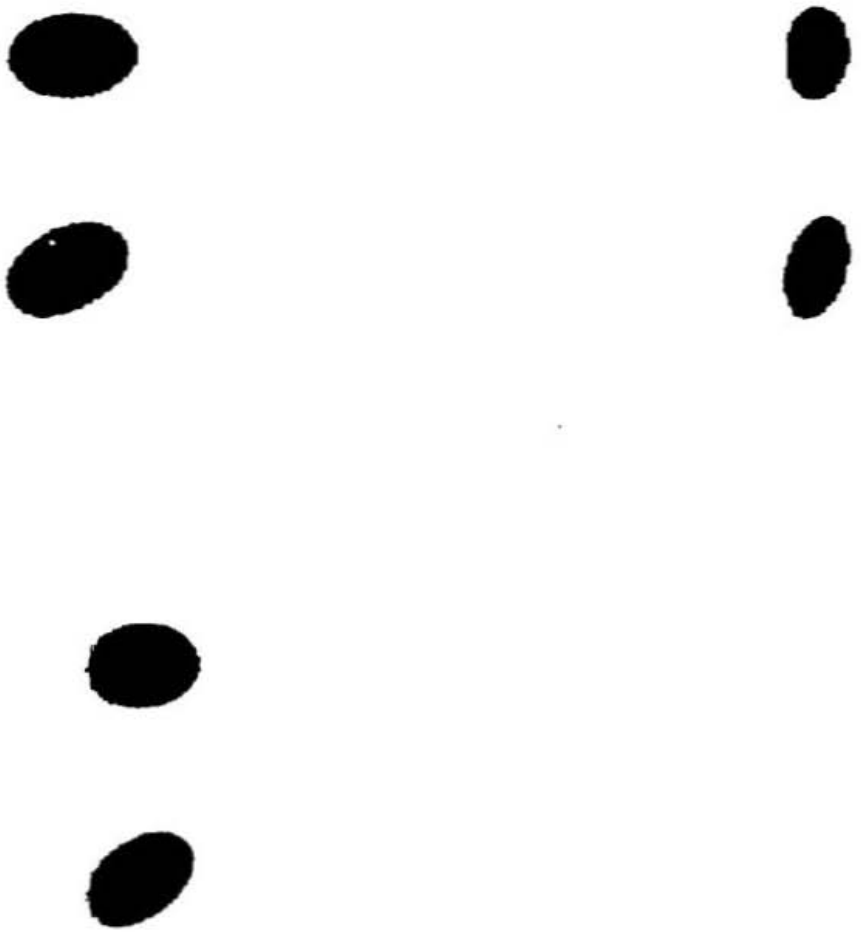

Figure 9: Radionuclide images of the two models.

Each image from the $\gamma$ camera (elliptic in shape) was then analyzed to determine the major axis length ($\zeta_n$), minor axis length ($\xi_n$), and angle of rotation for the major axis from the horizontal base of the image ($\delta_n$). For each trial, there were three images analyzed in this fashion ($xy$, $zy$, and $x = -z$ planes). The measurements are given in Table 2.

Table 2: Measurements of axes lengths ($\zeta_n$ and $\xi_n$ in $cm$) and angle of rotation ($\delta_n$ in °) taken from each image.

| Trial # | $\zeta_1$ | $\xi_1$ | $\delta_1$ | $\zeta_2$ | $\xi_2$ | $\delta_2$ | $\zeta_3$ | $\xi_3$ | $\delta_3$ |
|---|---|---|---|---|---|---|---|---|---|
| 1 | 4.14 | 1.98 | 67 | 3.61 | 2.27 | 65 | 2.93 | 2.40 | -59 |
| 2 | 4.24 | 2.77 | -48 | 3.82 | 2.24 | -41 | 3.38 | 2.27 | -14 |
| 3 | 4.16 | 2.62 | 32 | 4.14 | 2.18 | 23 | 4.01 | 2.15 | 12 |
| 4 | 4.07 | 2.38 | -6 | 4.11 | 1.99 | -9 | 4.11 | 2.44 | -9 |
| 5 | 4.05 | 2.77 | 86 | 3.71 | 2.81 | 82 | 2.88 | 2.10 | 3 |
| 6 | 4.14 | 2.75 | 67 | 3.83 | 2.61 | 55 | 3.22 | 2.06 | 20 |
| 7 | 4.09 | 2.66 | -60 | 3.68 | 2.77 | -59 | 3.22 | 2.13 | 12 |
| 8 | 4.20 | 2.12 | 84 | 3.92 | 2.02 | 76 | 3.15 | 1.99 | 61 |
| 9 | 4.07 | 2.77 | -84 | 3.56 | 2.81 | -83 | 2.87 | 1.98 | 0 |
| 10 | 4.31 | 1.98 | 66 | 3.84 | 1.99 | 63 | 3.22 | 2.32 | 59 |
| 11 | 4.26 | 2.04 | 68 | 3.85 | 2.21 | 67 | 2.81 | 2.35 | -79 |
| 12 | 4.07 | 1.97 | -84 | 3.82 | 2.12 | -88 | 2.88 | 2.10 | 87 |
| 13 | 4.19 | 2.80 | 36 | 4.02 | 2.62 | 24 | 3.91 | 2.09 | 0 |
| 14 | 4.28 | 2.21 | -50 | 3.82 | 2.58 | -49 | 3.51 | 2.68 | 31 |
| 15 | 4.26 | 2.21 | -68 | 3.80 | 2.04 | 60 | 2.97 | 2.53 | -53 |
| 16 | 4.17 | 2.35 | 90 | 3.73 | 2.25 | 80 | 3.07 | 2.04 | 54 |
| 17 | 4.06 | 2.81 | -70 | 3.90 | 2.68 | -65 | 3.17 | 2.15 | -23 |
| 18 | 4.18 | 2.09 | 88 | 3.81 | 2.10 | -84 | 2.98 | 2.10 | -68 |
| 19 | 4.14 | 2.82 | -67 | 3.94 | 2.58 | -56 | 3.39 | 2.10 | -21 |
| 20 | 4.28 | 1.96 | 40 | 4.19 | 2.35 | 36 | 3.58 | 2.81 | 9 |

The measurements given in Table 2 were obtained by using an image processing software application program to view and analyze each image. Manually drawn borders were drawn over each image. The major and minor axes lengths were estimated by manually measuring the lengths using pixels with a conversion factor of 6.13 $mm$/pixel. The coordinates of the endpoints for each axes were also recorded and the angle of rotation was then estimated from these coordinates.

The nine measurements from each trial were then substituted into equation (78) using

equations (76), (62), and (58). The volume estimate and percentage discrepancy for each trial are given in Table 3. The percentage discrepancy was calculated by subtracting the actual volume from the estimated volume and then dividing by the actual volume. The actual volume was calculated using $V = \frac{4}{3}\pi abc$ where $a = 4.6\ cm$, $b = 2.9\ cm$, and $c = 1.8\ cm$.

Table 3: Volume estimation using Table 2 measurements. Actual volume is 100.6 $cm^3$.

| Trial # | Estimated Volume ($cm^3$) | Percentage Discrepancy |
|---|---|---|
| 1 | 99.9 | -0.7 |
| 2 | 105.8 | 5.2 |
| 3 | 101.6 | 1.0 |
| 4 | 95.2 | -5.3 |
| 5 | 95.5 | -5.0 |
| 6 | 104.8 | 4.2 |
| 7 | 94.1 | -6.4 |
| 8 | 108.3 | 7.7 |
| 9 | 92.5 | -8.1 |
| 10 | 105.3 | 4.7 |
| 11 | 94.3 | -6.2 |
| 12 | 99.5 | -1.1 |
| 13 | 106.5 | 5.8 |
| 14 | 113.8 | 13.2 |
| 15 | 114.5 | 13.9 |
| 16 | 108.6 | 8.0 |
| 17 | 104.3 | 3.7 |
| 18 | 108.4 | 7.8 |
| 19 | 113.1 | 12.4 |
| 20 | 101.4 | 0.8 |

From Table 3, it can be seen that this method can be used to estimate the left ventricular volume (using an ellipsoid model). One problem that should be noted is that it may be difficult to determine the exact location of the left ventricular projection border

because of scattering and the pixel size (resolution of 6.13 $mm$/pixel). This will, of course, affect the volume estimates. This problem can be minimized by selecting a certain count threshold to help determine where the left ventricular border is located.

Another problem associated with the left ventricular border location is the interference of radiation from other organs. But, it must be kept in mind that the entire border outline is not needed. Only the endpoints of the major and minor axes are required for this volume estimation method. Any interference from radiation from other organs will have a much greater impact on any *count* based method of volume estimation, as opposed to our geometric method.

The total counts observed for each elliptical image were also recorded (Table 4). Since the counts were recorded for a period of two minutes for each image, they should be approximately equal. Because of self attenuation, the counts were observed to differ by as much as 33.7% for images within the same trial. Note that the counts decreased from trial to trial because of its decay rate. $^{99m}Tc$ has a half life of six hours while the elapsed time from trial 3 to trial 20 was approximately one hour and twenty minutes. Trials 1 and 2 were performed on a separate occasion using a different concentration of radionuclide, thus a different count rate. Also, the odd numbered trials between 3 and 19 (inclusive) were performed with one model while the even numbered trials between 4 and 20 (inclusive) were performed with the other model, containing a different concentration.

Table 4: Total counts under each elliptical image without any adjustment for radioactive decay.

| Trial # | Image 1 | Image 2 | Image 3 | Maximum % Increase |
|---|---|---|---|---|
| 1 | 259714 | 252095 | 231387 | 12.2 |
| 2 | 471028 | 413820 | 398161 | 18.3 |
| 3 | 316445 | 288374 | 278726 | 13.5 |
| 4 | 325422 | 300030 | 304599 | 8.5 |
| 5 | 308332 | 298598 | 237378 | 29.9 |
| 6 | 322348 | 311866 | 264528 | 21.9 |
| 7 | 300896 | 291368 | 246196 | 22.2 |
| 8 | 298124 | 284618 | 246128 | 21.1 |
| 9 | 298542 | 284655 | 223315 | 33.7 |
| 10 | 287302 | 271971 | 254767 | 12.8 |
| 11 | 266867 | 256722 | 233307 | 14.4 |
| 12 | 276079 | 263858 | 235043 | 17.5 |
| 13 | 287380 | 277053 | 248297 | 15.7 |
| 14 | 280115 | 285915 | 276856 | 3.3 |
| 15 | 261447 | 240377 | 230727 | 13.3 |
| 16 | 281608 | 268655 | 225830 | 24.7 |
| 17 | 273940 | 266471 | 218320 | 25.5 |
| 18 | 270438 | 256222 | 220341 | 22.7 |
| 19 | 268446 | 260362 | 217265 | 23.6 |
| 20 | 259883 | 266432 | 277537 | 6.8 |

If a count based left ventricular volume estimation method was performed on this same set of images, then there would be a relatively large discrepancy among the volume estimates. To perform a count based procedure, a thin walled (for minimal self attenuation) test sample would also have to be imaged under the gamma camera for the same period of time as the images. By measuring the volume of this sample, a factor of volume/count can be estimated and then applied to the data of Table 4 to obtain volume estimates. Because the counts varied for images within the same trial, then the volume estimates from each of

the three images within the same trial would also vary by the same percentages. Thus, the percentages given in the last column of Table 4 would represent the percentage discrepancy among the volume estimates using a count based method. These percentages would be even higher if the decay rate of $^{99m}Tc$ was not taken into consideration properly. This confirms that self attentuation can be a major problem in count based methods.

In a more practical situation, there would also be attenuation due to other organs and bones. Thus, the volume estimates from a count based method would also have inherent errors due to these factors as well. Because of so many factors such as attenuation, self attenuation, radioactive decay, scattering, and interference from other organs, it would appear as though count based methods would not be able to estimate accurately the volume of the left ventricle.

The major problem of using a geometric method of volume estimation is how well the geometric model fits the actual organ. For most cases, an ellipsoidal model does seem to be a relatively accurate model (Davila and Sanmarco, 1966) but abnormalities in the left ventricle will affect the accuracy of this method. The extent of this error would depend upon how the abnormality affects the overall left ventricular volume and shape of the images. Another problem associated with geometric methods is the estimation of the left ventricular border (actually, only the location of the major and minor axes endpoints need to be known). The impact of this problem can be minimized by using a threshold count to help determine the border location. Also, a scaling factor can be determined experimentally to reduce the effect of scattering.

# Chapter 4:
# Conclusions

Using measurements taken from three images has been shown to be an effective method of volume estimation for an ellipsoidal model. Data from only two projections is not always sufficient. There are several shortcomings associated with this method. First of all, if the left ventricle is abnormal in shape, then an ellipsoidal model may not be an accurate representation. In this case, a count based method may be more accurate since it does not take into consideration the shape of the imaged object. But, it must be kept in mind that the problems of using a count based method still have to be overcome in order to obtain acceptably accurate results.

Another shortcoming of using the ellipsoidal model approach is that care must be taken to determine the left ventricular border in each image. Any error in estimating the location of the border will result directly in an error in the volume estimate.

It should be mentioned that this method of volume estimation has not yet been applied to humans. Some problems that may arise include camera location and interference from other organs. This method relies on the camera being located in a fixed arbitrary reference coordinate system. After the first image is complete, the camera should be rotated 45° to obtain the image in the third projection plane ($x = -z$ plane). Finally, the camera must be rotated by another 45° in the same direction as the first 45° rotation, to obtain the image in the second projection plane ($zy$ plane). Obviously, any error in the rotation direction or rotation angle will cause an error in the volume estimate. The impact of this

problem can be minimized by ensuring that the camera location is carefully monitored and checked to ensure accurate camera placement.

Another problem that may arise is the possible interference from other organs. It may be difficult to find three views, separated by 45° each, that show the left ventricle without any overlap of radiation from other organs. Of course, if the left ventricle is not abnormal in shape, then the border can still be estimated if there is only a small portion of overlap (extrapolate the border location) or if the counts from another organ are sufficiently small allowing the border to be easily recognizable. If a count based method were used, any overlap would not be acceptable since the extra counts would directly affect the accuracy of the volume estimate.

Once the three images have been formed and processed then another problem arises which is inherent to all methods. The true volume is not known and thus the accuracy of this method would also be unknown. Of course, there are other methods of left ventricular volume estimation available but there would be some uncertainty about using these estimates as the true volume. The most accurate method, as accepted by most physicians, could be used as a reference but it must be kept in mind that the reference method will have some degree of error associated with it.

Even though this ellipsoidal method of volume estimation was developed for human hearts, it was good to test initially this method using an ellipsoidal model. Knowing the true volume helped give a better indication of the accuracy of this method. Also, the effects of self attenuation have been shown to be considerable.

# Chapter 5:
# Recommendations

There are several recommendations that could improve the approach discussed in this thesis. To account for any systematic errors in estimating the location of the left ventricular border, a correction scaling factor or an improved border location technique could be implemented. A more accurate location of the left ventricular border can also be determined by either having a more skilled analyst process the images or by using a computer algorithm to detect the border.

This ellipsoidal model method can be improved by using the counts in addition to the measurements of axes lengths and angle of rotation. The nine measurements from each trial can be used to estimate the dimensions of each axis ($a$, $b$, and $c$) and the angles of rotation ($\alpha$, $\beta$, and $\gamma$). From this information, the depth and volume underneath each pixel can be calculated. Next, the self attenuation can be accounted for and an estimate of the counts, underneath each pixel, can be calculated. This theoretical estimate can be compared to the actual measured value. This comparison can then be used to alter the volume estimate to account for abnormalities. Thus, a combination of the geometric and count based methods may be the best alternative to estimate the volume of the left ventricle.

It is also recommended that the effects of self attenuation should be more closely examined. By placing the model in a known orientation ($\alpha$, $\beta$, and $\gamma$ are known), then the exact volume under each pixel can be calculated and compared with the measured

result. From this, a more accurate representation (from a practical perspective) of self attenuation can be obtained which can then be used to improve this method or even count based methods.

# Glossary

angiocardiography

The roentgenographic visualization of the heart and its blood vessels after injection of a radiopaque substance.

caudal tilt

A tilt towards the hind part of the body or object.

cineangiography

A series of roentgenographic images of the blood vessels after injection of a radiopaque substance.

echocardiography

The recording of an ultrasound image of the heart. A transducer, usually placed on the chest wall, transmits very high frequency waves that are reflected from tissue interfaces.

Fick technique

A technique developed by Adolf Fick to calculate the cardiac output from the measurement of the minute volume of oxygen consumption.

first pass kinetics

The study of a radioisotope as it passes through an organ for the first time.

fluoroscopy

The observation of an opaque object (organ) by the means of the shadow cast by the object onto a fluorescent screen with a radioisotope source placed behind the object.

gated equilibrium studies

A series of images created by the measurement of counts separated within the cardiac cycle.

radiopaque

Being opaque to X rays or other forms of radiation.

roentgenographic

Photography made with X rays (radiograph).

scintigraphy

A diagnostic technique in which a two dimensional picture of a bodily radiation source is obtained by the use of radioisotopes.

thermodilution

A technique for measuring blood flow by the introduction of a relatively cold fluid of known quantity into a circulation. By measuring the fall in temperature by a themistor. the volume in which the cold fluid has been diluted can be calculated.

ventriculography

The art of making an X ray photograph of the ventricles made after withdrawing fluid and replacing it with air or a radiopaque substance.

# References


Albert A. (1949). *Solid Analytic Geometry*. (First Edition). The Maple Press Company. 116-117 p.

Al-Khawaja I.M., Lahiri A., and Raftery E.B. (1988). Measurement of Absolute Left Ventricular Volume by Radionuclide Angiography: A Technical Review. *Nucl Med Comm*; **9**: 495-504.

Arvidsson H. (1958). Angiocardiographic Observations in Mitral Disease, With Special Reference to the Volume Variations in the Left Atrium. *Acta Radiol* (suppl); **158**: 1-124.

Ashburn W.L., Schelbert H.R., and Verba J.W. (1978). Left Ventricular Ejection Fraction - A Review of Several Radionuclide Angiographic Approaches Using the Scintillation Camera. *Prog Cardiovasc Dis*: **20**: 267-284.

Aurigemma G.P., Gaasch W.H., Villegas B., and Meyer T.E. (1995). Noninvasive Assessment of Left Ventricular Mass, Chamber Volume, and Contractile Function. *Curr Probl Cardiol*: **20**: 363-440.

Berman D.S., Salel A.F., DeNardo G.L., Bogren H.G., and Mason D.T. (1975). Clinical Assessment of Left Ventricular Regional Contraction Patterns and Ejection Fraction by High-Resolution Gated Scintigraphy. *J Nucl Med*; **16**: 865-874.

Boström P.Å., Hemdal B., Ahlgren L., Svensson M., Lecerof H., and Lilja B. (1987).

Radionuclide Left Ventricular Volume Determination. Influence of Scattered Radiation and Surrounding Activity. *Clin Physiol*; **7**: 303-312.

Burns R.J., Nitkin R.S., Weisel R.D., Houle S., Prieur T.G., McLaughlin P.R., and Druck M.N. (1985). Optimized Count-Based Scintigraphic Left Ventricular Volume Measurement. *Can J Cardiol*; 1: 42-46.

Burns R.J., Druck M.N., Woodward D.S., Houle S., and McLaughlin P.R. (1983). Repeatability of Estimates of Left-Ventricular Volume from Blood-Pool Counts: Concise Communication. *J Nucl Med*; **24**: 775-781.

Burow R.D., Wilson M.F., Heath P.W., Corn C.R., Amil A., and Thadani U. (1982). Influence of Attenuation on Radionuclide Stroke Volume Determinations. *J Nucl Med*; **23**: 781-785.

Chin B.B., Bloomgarden D.C., Xia W., Kim, H.J., Fayad Z.A., Ferrari V.A., Berlin J.A., Axel L., and Alavi A. (1997). Right and Left Ventricular Volume and Ejection Fraction by Tomographic Gated Blood-Pool Scintigraphy. *J Nucl Med*; **38**: 942-948.

Clements I.P., Brown M.L., and Smith H.C. (1981). Radionuclide Measurement of Left Ventricular Volume. *Mayo Clin Proc*; **56**: 733-739.

Clements I.P., Sinak L.J., Gibbons R.J., Brown M.L., and O'Connor M.K. (1990). Determination of Diastolic Function by Radionuclide Ventriculography. *Mayo Clin Proc*; **65**: 1007-1019.

Coffey J.L., Cristy M., and Warner G. (1981). Specific Absorbed Fractions for Photon

Sources Uniformly Distributed in the Heart Chambers and Heart Wall of a Heterogeneous Phantom. *J Nucl Med*; **22**: 65-71.

Davila J.C. and Sanmarco M.E. (1966). An Analysis of the Fit of Mathematical Models Applicable to the Measurement of Left Ventricular Volume. *The Am J Cardiol*; **18**: 31-42.

Dehmer G.J., Lewis S.E., Hillis L.D., Twieg D., Falkoff M., Parkey R.W., and Willerson J.T. (1980). Nongeometric Determination of Left Ventricular Volumes From Equilibrium Blood Pool Scans. *The Am J Cardiol*; **45**: 293-300.

Dehmer G.J., Firth B.G., Lewis S.E., Willerson J.T., and Hillis L.D. (1981). Direct Measurement of Cardiac Output by Gated Equilibrium Blood Pool Scintigraphy: Validation of Scintigraphic Volume Measurements by a Nongeometric Technique. *Am J Cardiol*; **47**: 1061-1067.

Dodge H.T., Hay R.E., and Sandler H. (1962). An Angiocardiographic Method for Directly Determining Left Ventricular Stroke Volume in Man. *Circ Res*; **11**: 739-745.

Dodge H.T., Sandler H., Ballew D.W., and Lord J.D. (1960). The Use of Biplane Angiocardiography for the Measurement of Left Ventricular Volume in Man. *Am Heart J*; **60**: 762-776.

Eckelman W.C., Smith T.D., and Richards P. (1976). Labelling Blood Cells with Tc-99m. In *Radiopharmaceuticals*. Justa M.G., Rhodes B.A., Cooper J.F., and Sodd V.J., eds. The Society of Nuclear Medicine; 49-54.

Fearnow E.C., Stanfield J.A., Jaszczak R.J., Harris C.C., and Coleman R.E. (1985). Factors Affecting Ventricular Volumes Determined by a Count-Based Equilibrium Method. *J Nucl Med*; **26**: 1042-1047.

Graham T.P. (Jr.), Jarmakani J.M., Canent R.V. (Jr.), and Morrow M.N. (1971). Left Heart Volume Estimation in Infancy and Childhood. *Circulation*; **43**: 895-904.

Graham T.P. (Jr.), Jarmakani J.M., Atwood G.F., and Canent R.V. (Jr.) (1973). Right Ventricular Volume Determination in Children. *Circulation*; **47**: 144-153.

Greene D.G., Carlisle R., Grant C., and Bunnell I.L. (1967). Estimation of Left Ventricular Volume by One-Plane Cineangiography. *Circulation*; **35**: 61-69.

Harpen M.D., Dubuisson R.L., Head G.B., Parmley L.F., Jones T.B., and Robinson A.E. (1983). Determination of Left-Ventricular Volume from First-Pass Kinetics of Labeled Red Cells. *J Nucl Med*; **24**: 98-103.

Harris C.C., Greer K.L., Jaszczak R.J., Floyd C.E. (Jr.), Fearnow E.C., and Coleman R.E. (1984). Tc-99m Attenuation Coefficients in Water-Filled Phantoms Determined with Gamma Cameras. *Med Phys*; **11**: 681-685.

Hillis L.D., Winniford M.D., Dehmer G.J., and Firth B.G. (1984). Left Ventricular Volumes by Single-Plane Cineangiography: In Vivo Validation of the Kennedy Regression Equation. *Am J Cardiol*; **53**: 1159-1163.

Høilund-Carlsen P.F., Marving J., Rasmussen S., Haunsø S., and Pedersen J.F. (1984). Accuracy of Absolute Left Ventricular Volumes and Cardiac Output Determined by

Radionuclide Cardiography. *Int J Cardiol*; **6**: 505-521.

Hutton B.F., Bautovich G.J., and Cormack J. (1981). Determination of Absolute Cardiac Ventricular Volume Using Radionuclide Techniques, *Phys Med Biol*; **26**: 715-718.

Iskandrian A.S., Hakki A.H., Kane S.A., and Segal B.L. (1981). Quantitative Radionuclide Angiography in Assessment of Hemodynamic Changes During Upright Exercise: Observations in Normal Subjects, Patients with Coronary Artery Disease and Patients with Aortic Regurgitation. *Am J Cardiol*; **48**: 239-246.

Jaszczak R.J., Morris K.G., Cobb F.R., and Coleman R.E. (1980). Left Ventricular Volume from Multigated Blood Pool Data Using Attenuation Correction (abstract). *Med Phys*; **7**: 423.

Keller A.M., Simon T.R., Smitherman T.C., Malloy C.R., and Dehmer G.J. (1987). Direct Determination of the Attenuation Coefficient for Radionuclide Volume Measurements. *J Nucl Med*; **28**: 102-107.

Kennedy J.W., Trenholme S.E., and Kasser I.S. (1970). Left Ventricular Volume and Mass from Single-Plane Cineangiocardiogram. A Comparison of Anteroposterior and Right Anterior Oblique Methods. *Am Heart J*; **80**: 343-352.

Koral K.F., Rabinovitch M.A., Kalff V., Chan W., Juni J.E., Lerman B., Lampman R., Walton J., Vogel R., Pitt B., and Thrall J.H. (1985). Variations on Calculating Left-Ventricular Volume with the Radionuclide Count-Based Method. *Med Phys*; **12**:

93-98.

Lewis S.E., Dehmer G.J., Falkoff M., Hillis L.D., and Willerson J.T. (1979). A Non-Geometric Method for the Scintigraphic Determination of Left Ventricular Volume: Contrast Correlation (abstract). *J Nucl Med*; **20**: 661.

Links J.M., Becker L.C., Shindledecker J.G., Guzman P., Burow R.D., Nickoloff E.L., Alderson P.O., and Wagner H.N. (1982). Measurement of Absolute Left Ventricular Volume From Gated Blood Pool Studies. *Circulation*; **65**: 82-91.

Longmore D.B., Underwood S.R., Hounsfield, Bland C., Poole-Wilson P.A., Denison D., Klipstein R.H., Firmin D.N., Watanabe M., Fox K., Rees R.S.O., McNeilly A.M., and Burman E.D. (1985). Dimensional Accuracy of Magnetic Resonance in Studies of the Heart. *Lancet*; **1**: 1360-1362.

Mahmarian J.J., Moye L., Verani M.S., Eaton T., Francis M., and Pratt C.M. (1991). Criteria for the Accurate Interpretation of Changes in Left Ventricular Ejection Fraction and Cardiac Volumes as Assessed by Rest and Exercise Gated Radionuclide Angiography. *J Am Coll Cardiol*; **18**: 112-119.

Massardo T., Gal R.A., Grenier R.P., Schmidt D.H., and Port S.C. (1990). Left Ventricular Volume Calculation Using a Count-Based Ratio Method Applied to Multigated Radionuclide Angiography. *J Nucl Med*; **31**: 450-456.

Massie B.M., Kramer B.L., Gertz E.W., and Henderson S.G. (1982). Radionuclide Measurement of Left Ventricular Volume: Comparison of Geometric and Counts-

Based Methods. *Circulation*; **65**: 725-730.

Maurer A.H., Siegel J.A., Denenberg B.S., Carabello B.A., Gash A.K., Spann J.F. and Malmud L.S. (1983). Absolute Left Ventricular Volume from Gated Blood Pool Imaging with Use of Esophageal Transmission Measurement. *Am J Cardiol*; **51**: 853-858.

Melin J.A., Wijns W., Robert A., Nannan M., Coster P.D., Beckers C., and Detry J.M. (1985). Validation of Radionuclide Cardiac Output Measurements During Exercise. *J Nucl Med*; **26**: 1386-1393.

Nichols K., Adatepe M.H., Isaacs G.H., Powell O.M., Pittman D.E., Gay T.C., and Begg F.R. (1984). A New Scintigraphic Method for Determining Left Ventricular Volumes. *Circulation*; **70**: 672-680.

Nickel O., Schad N., Andrews E.J. (Jr.), Fleming J.W., and Mello M. (1982). Scintigraphic Measurement of Left-Ventricular Volumes from the Count-Density Distribution. *J Nucl Med*; **23**: 404-410.

Nickoloff E.L., Perman W.H., Esser P.D., Bashist B., and Alderson P.O. (1984). Left Ventricular Volume: Physical Basis for Attenuation Corrections in Radionuclide Determinations. *Radiology*; **152**: 511-515.

Parrish M.D., Graham T.P. (Jr.), Born M.L., Jones J.P., Boucek R.J., and Partain C.L. (1982). Radionuclide Ventriculography for Assessment of Absolute Right and Left Ventricular Volumes in Children. *Circulation*; **66**: 811-819.

Pattynama P.M.T., DeRoos A., Van der Wall E.E., and Van Voorthuisen A.E. (1994). Evaluation of Cardiac Function with Magnetic Resonance Imaging. *Am Heart J*: **128**: 595-607.

Petru M.A., Sorensen S.G., Chaudhuri T.K., Rosen P., and O'Rourke R.A. (1984). Attenuation Correction of Equilibrium Radionuclide Angiography for Noninvasive Quantitation of Cardiac Output and Ventricular Volumes. *Am Heart J*; **107**: 1221-1228.

Phillips R.E. and Feeney M.K. (1990). *The Cardiac Rhythms: A Systematic Approach to Interpretation*, (Third Edition), W.B. Saunders Company, Philadelphia, PA, 19106-3399, 591 p.

Rabinovitch M.A., Kalff V., Koral K., Chan W., Juni J.E., Lerman B., Lampman R., Walton J., Grassley D., Vogel R., Pitt B., and Thrall J.H. (1984). Count-Based Left Ventricular Determination Utilizing a Left Posterior Oblique View for Attenuation Correction. *Radiology*; **150**: 813-818.

Rackley C.E. (1976). Quantitative Evaluation of Left Ventricular Function by Radiographic Techniques. *Circulation*; **54**: 862-879.

Ryo U.Y., Mohammadzadeh A.A., Siddiqui A., Columbetti L.G., and Pinsky S.M. (1976). Evaluation of Labeling Procedures and In Vivo Stability of $^{99m}Tc$ Red Blood Cells. *J Nucl Med*; **17**: 133-136.

Sandler H. and Dodge H.T. (1968). The Use of Single Plane Angiocardiograms for the Calculation of Left Ventricular Volume in Man, *Am Heart J*; **75**: 325-334.

Sapin P.M., Schroeder K.D., Smith M.D., DeMaria A.N., and King D.L. (1993). Three-Dimensional Echocardiographic Measuremment of Left Ventricular Volume In Vitro: Comparison With Two-Dimensional Echocardiography and Cineventriculography. *J Am Coll Cardiol*: **22**: 1530-1537.

Schwaiger M., Ratib O., Henze E., Grossman R., Dracup K., Tillisch J.H., Bae J.H., and Schelbert H.R. (1984). Left Ventricular Stroke Volume Determinations from Radionuclide Ventriculograms: The Effects of Photon Attenuation. *Radiology*; **153**: 235-240.

Seiderer M., Bohn I., Buell U., Kleinhans E., and Strauer B.E. (1983). Influence of Background and Absorption Correction on Nuclear Quantification of Left Ventricular End-Diastolic Volume. *Br J Radiol*: **56**: 183-187.

Seldin D.W., Esser P.D., Nichols A.B., Ratner S.J., and Alderson P.O. (1983). Left Ventricular Volume Determined from Scintigraphy and Digital Angiography by a Semi-Automated Geometric Method. *Radiology*; **149**: 809-813.

Sherwood L. (1993). *Human Physiology: From Cells to Systems*, (Second Edition), West Publishing Company, St. Paul, MN, 55164-0526, 745 p.

Siegel J.A., Maurer A.H., Wu R.K., Blasius K.M., Denenberg B.S., Gash A.K., Carabello B.A., Spann J.F., and Malmud L.S. (1984). Absolute Left Ventricular Volume by an Iterative Build-Up Factor Analysis of Gated Radionuclide Images. *Radiology*; **151**: 477-481.

Simon T.R., Dowdey J.E., Lipscomb K.M., and Smitherman T.C. (1985). Correlation of Scintigraphy and Angiography for Ventricular Volume Determinations using Realistic Cardiac Phantoms: The Unimportance of Self-Attenuation. *Radiology*; **154**: 232-233.

Slutsky R., Karliner J., Ricci D., Kaiser R., Pfisterer M., Gordon D., Peterson K., and Ashburn W. (1979). Left Ventricular Volumes by Gated Equilibrium Radionuclide Angiography: A New Method. *Circulation*; **60**: 556-564.

Slutsky R., Battler A., Gerber K., Gordon D., Verba J., Peterson K., Murray I.P., and Ashburn W. (1980). A Simplified Method for the Calculation of Left Ventricular Volume by Equilibrium Radionuclide Angiography. *Cathet Cardiovas Diag*; **6**: 49-60.

Slutsky R.A. (1983). On the Analysis of Left Ventricular Volume from Gated Radionuclide Ventriculograms (editorial note). *Chest*; **84**: 2-3.

Starling M.R., Dell'Italia L.J., Walsh R.A., Little W.C., Benedetto A.R., and Nusynowitz M.L. (1984a). Accurate Estimates of Absolute Left Ventricular Volumes from Equilibrium Radionuclide Angiographic Count Data Using a Simple Geometric Attenuation Correction. *J Am Coll Cardiol*; **3**: 789-798.

Starling M.R., Dell'Italia L.J., Nusynowitz M.L., Walsh R.A., Little W.C., and Benedetto A.R. (1984b). Estimates of Left-Ventricular Volumes by Equilibrium Radionuclide Angiography: Importance of Attenuation Correction. *J Nucl Med*; **25**: 14-20.

Strauss H.W., McKusick K.A., Boucher C.A., Bingham J.B., and Pohost G.M. (1979).

Of Linens and Laces - The Eighth Anniversary of the Gated Blood Pool Scan. *Semin Nucl Med*: **9**: 296-309.

Sullivan R.W., Bergeron D.A., Vetter W.R., Hyatt K.H., Haughton V., and Vogel J.M. (1971). Peripheral Venous Scintillation Angiocardiography in Determination of Left Ventricular Volume in Man. *Am J Cardiol*: **28**: 563-567.

Thomsen J.H., Patel A.K., Rowe B.R., Hellman R.S., Kosolcharoen P., Feiring A.J., Filipek T., Halama J.R., and Polcyn R.E. (1983). Estimation of Absolute Left Ventricular Volume from Gated Radionuclide Ventriculograms. *Chest*; **84**: 6-13.

Verani M.S., Gaeta J., LeBlanc A.D., Poliner L.R., Phillips L., Lacy J.L., Thornby J.I., and Roberts R. (1985). Validation of Left Ventricular Volume Measurements by Radionuclide Angiography. *J Nucl Med*; **26**: 1394-1401.

Wynne J., Green L.H., Mann T., Levin D., and Grossman W. (1978). Estimation of Left Ventricular Volumes in Man from Biplane Cineangiograms Filmed in Oblique Projections. *Am J Cardiol*: **41**: 726-732.